Swiss Journal of Geosciences (2018) 111:317–340
https://doi.org/10.1007/s00015-017-0294-z

Bristen granite: a highly differentiated, fluorite-bearing A-type granite from the Aar massif, Central Alps, Switzerland

Kurt Bucher[1] · Ulrike Seelig[1,2]

Received: 26 April 2017 / Accepted: 19 December 2017 / Published online: 9 February 2018

Abstract
Bristen granite is a body of fine-grained leucogranite occurring in the Gotthard rail base tunnel in the Central Alps. During construction of the tunnel, Bristen granite (Brgr) has been drilled along a 600 m long section. The aplite-granite belongs to the suite of Variscan granitoid intrusions of the Aar massif and contains a variety of accessory minerals typical of highly differentiated granites. Rock forming fluorite, partly enriched in yttrium (Y) and rare earth elements (REE), is intergrown with the late Y- and REE-bearing carbonate mineral synchysite. The granite contains a variety of Ti- and Y-REE-niobates, thorite, and zircon. Compared with the calc-alkaline central Aar granite (cAgr), Bristen granite is strongly depleted in Ti, P, Mg, Sr, and Ba and shows a remarkable enrichment in incompatible elements such as Rb, Th, U, Nb, Y, HREE and F. Bristen granite is the most evolved granitoid rock of the Aar massif. The composition of Brgr is typical of post-collisional reduced (ferroan) A-type granites. The Brgr melt formed in the lower crust and crystallized from a highly differentiated melt at the cotectic point in the quartz-feldspar system close to 100 MPa and 700 °C. The Brgr intruded as a small isolated stock pre-Variscan gneisses with sharply discordant contacts. The primary igneous host of Nb, Ta, Y, U, Th and REE is biotite in addition to minor amounts of allanite, and zircon. The presence of Y-REE-fluorite, synchysite, parisite and Y- and Ti-niobates and other REE-minerals can be related to reaction of igneous biotite and primary fluorite with hydrothermal fluids. The reaction is associated with alpine metamorphism, because Y-bearing fluorite and synchysite have been reported from Alpine fissures. The transformation of primary biotite to chlorite and muscovite released the heavy metal oxides under lower greenschist facies conditions that formed the Alpine diagnostic mineral stilpnomelane at about 300 °C.

Keywords Bristen granite · Aar massif · Fluorite · Synchysite · REE niobates

1 Introduction

Variscan granites form an essential component of the central European continental crust. The granite plutons and batholiths have been emplaced in predominantly gneissic crystalline basement of Variscan, Caledonian and older age. Examples of this setting are the Black Forest Mountains (McCann et al. 2008; Geyer et al. 2011), the Vosges Mountains and the Massif Central (Keppie 1994; McCann et al. 2008), the Erzgebirge (Förster et al. 1999) in central Europe and Sardinia in southern Europe (Conte et al. 2017). This Variscan crystalline basement is exposed in the northern part of the Alps in erosion windows called "external crystalline massifs" (ECM). The largest exposed ECM is the Aar massif (Fig. 1). A number of granitoid intrusive bodies of Variscan age (Pfiffner 2014) form the glaciated high mountains of the Aar massif. The largest and most prominent granite is the central Aar granite (cAgr), which extends for more than 90 km in SW–NE direction (Fig. 1). The granite has a number of lobes and satellite intrusions of overall granitoid composition with small, though distinct compositional variations (Schaltegger 1994; Labhart 2005).

Editorial Handling: E. Gnos.

✉ Kurt Bucher
bucher@uni-freiburg.de

Ulrike Seelig
u.seelig@fz-juelich.de

[1] Institute of Mineralogy and Petrology, University of Freiburg, Albertstr. 23b, 79104 Freiburg, Germany

[2] Present Address: Projektträger Jülich (ptj), Forschungszentrum Jülich GmbH, Zimmerstr. 26-27, 10969 Berlin, Germany

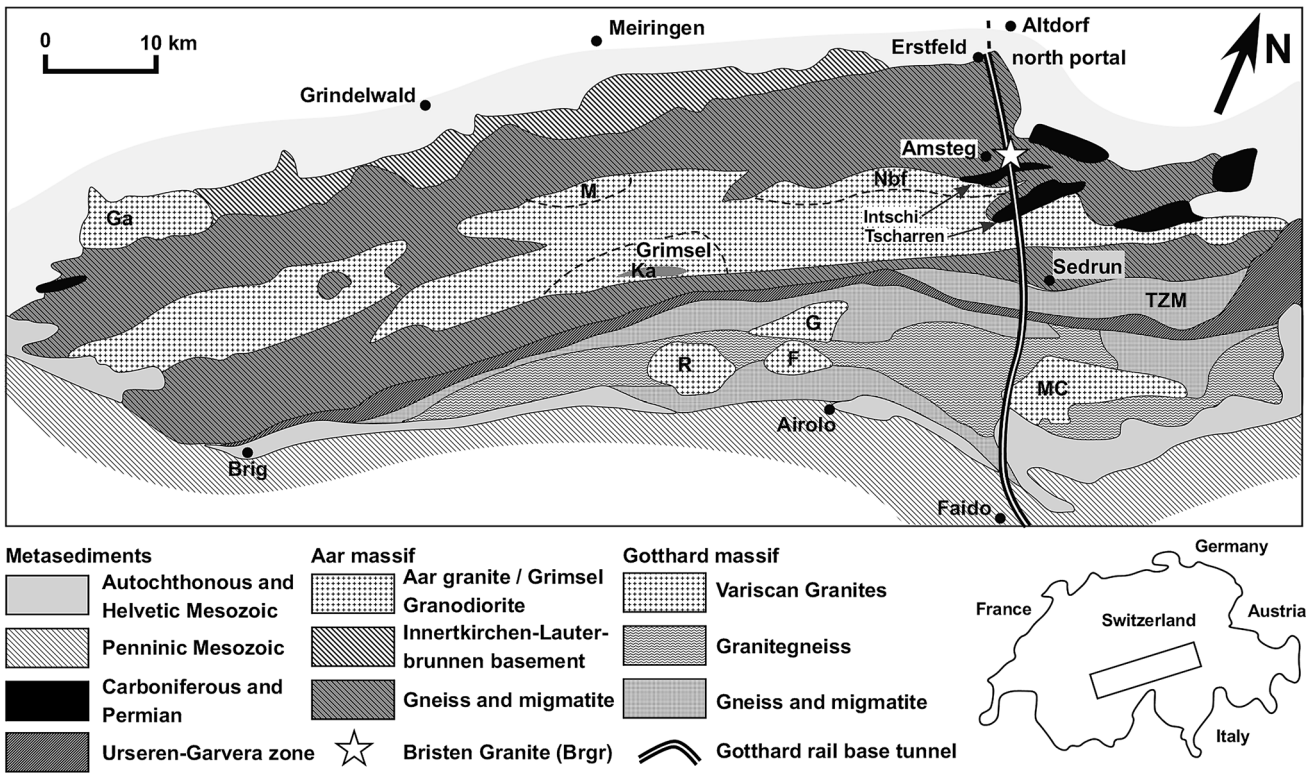

Fig. 1 Geological map of the basement windows: Aar massif north of the Urseren-Garvera Zone, Gotthard massif south of the Urseren-Garvera Zone, and Tavetsch (TZM) massif (redrawn after Labhart 2005). Location of Bristen granite (Brgr) at tunnel level is marked with a star, its extent is unknown. Variscan granites: *F* Fibbia, *G* Gamsboden, *Ga* Gastern, *Gr* Grimsel granodiorite, *M* Mittagflue, *MG* Medel granite, *Nbf* northern border facies of central Aar granite, *R* Rotondo, *Ka* Kessiturm aplite. Metavolcanic rocks (metarhyolites) of Intschi Formation and Tscharren Formation

An exceptional leucogranite belonging to the Aar massif has been located in 2002 during the drilling operations for the Gotthard rail base tunnel through the central Alps. The granite is situated under the village of Bristen in the Maderan valley and is therefore named Bristen granite (Brgr). The Maderan valley joins the main Reuss valley at the village of Amsteg (Fig. 1). The Bristen granite is an extremely differentiated granite with rock-forming fluorite and various Nb-, Y- and REE-bearing minerals. This paper describes Brgr for the first time in some detail and presents rock composition data including trace- and REE-element data, textural data and mineral composition data. The data suggest that Brgr formed from a melt typical of A-type granites at low pressure and contained igneous REE-bearing biotite. The data suggest furthermore that Alpine greenschist facies overprint converted Variscan biotite to chlorite and a variety of secondary REE-bearing carbonates and oxides.

2 The tunnel and the occurrence of Bristen granite

The Gotthard rail base tunnel has been completed in 2015 and started operation in the fall of 2016. It is the longest rail tunnel in the world (57 km). The tunnel has been drilled in different sections mostly with tunnel boring machines. The Amsteg section is 11.35 km long (Figs. 1 and 2); its base is about 500 m above sea level (a.s.l.). The distance of the base tunnel at 500 m a.s.l. to the surface varies between 305 and 2130 m (maximum depth near Chrüzlistock peak 2707 a.s.l.). The position in the tunnel is given with reference to the north portal near Erstfeld = 0 Tm (Tm = tunnel meters). The notation of Alptransit NEAT, the contractor, includes a prefix 1 for samples from the east tube and a 2 for the west tube. A sample from Tm km 8.362 in the east tube has its NEAT position given by 108362. All samples studied in this paper have been collected in the east-tube thus the position notation has been simplified to Tm in km. The Bristen granite occurs between Tm = 8.362 km and 8.967 km, that is for a distance of 605 m. Its depth below the surface varies from 305 to 355 m. The section through the Bristen granite has been drilled in 2002–2003. The N-S section along the tunnel is shown on Fig. 2. The E-W extent of the granite is unknown. However, the cross section (Fig. 2) suggests that the granite forms a small undeformed intrusive stock with sharp boundaries to the pre-Variscan gneisses including the Erstfeld Gneiss. Today, after the final lining and fitting of the tunnel, Bristen granite is no longer accessible.

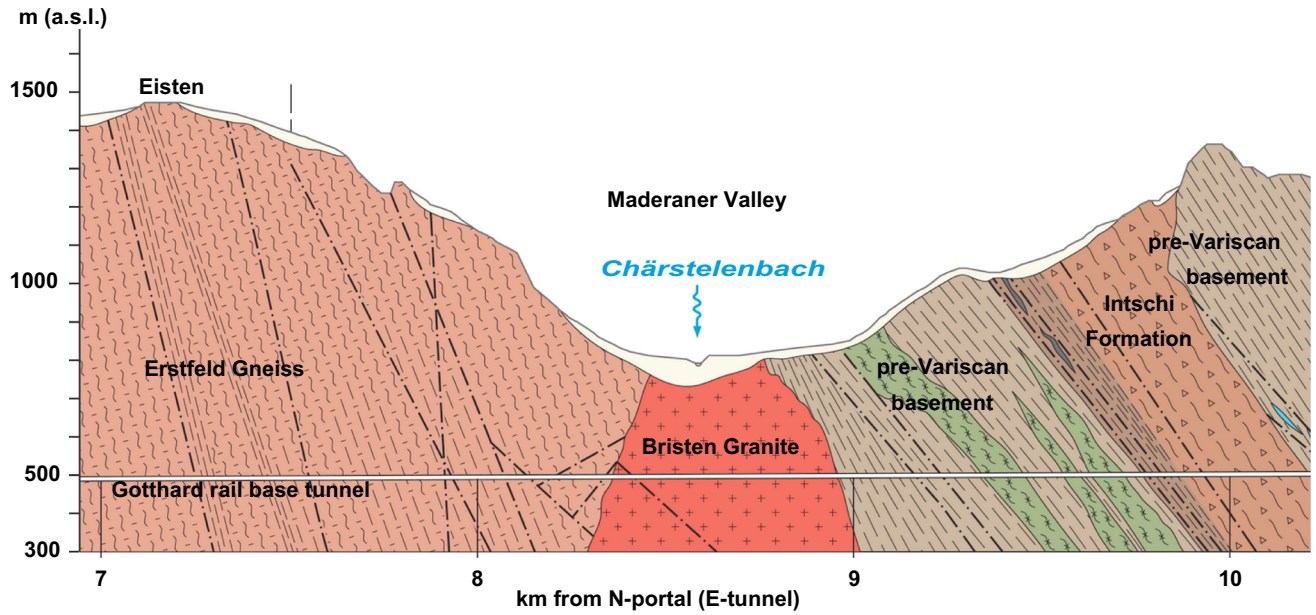

Fig. 2 Geological section along the Gotthard rail tunnel (Fig. 1) showing the location and setting of the Bristen granite (Guntli et al. 2016). The Intschi formation comprises Paleozoic metasediments and metarhyolites

3 Geological background

The Bristen granite is a part of the Aar massif (Fig. 1), which shows all characteristic features of continental basement (Pflugshaupt 1927; Hügi 1956; Abrecht and Schaltegger 1988; Schaltegger 1990, Schaltegger and Corfu 1992, 1995; Schaltegger 1993; von Raumer et al. 1999). The Variscan intrusives of the Aar massif include: Central Aar granite, Grimsel granodiorite, and Giuv syenite and many other smaller bodies such as Schöllenen syenite. The basement of the massif has been covered by a sedimentary sequence from the Carboniferous to the upper Jurassic. The Permo-Carboniferous sediments were deposited in local basins; from the Triassic the sediments completely cover the basement. The cover includes late Paleozoic rhyolites and volcaniclastic rocks (Intschi- and Tscharren-Formation along the tunnel section). The Jurassic Malm limestone is the most prominent member (several hundred meters thickness) of this sequence. The cover remained autochthonous to the basement during Alpine deformation in the northern part of the massif. The pre-Mesozoic history of the Aar massif (Schaltegger 1994) and the source of granitic magmatism (Schaltegger and Corfu 1992, 1995) have been studied in detail. Other aspects of Aar massif geology have been reported and discussed (e.g.) in Mercolli and Oberhänsli (1988, Oberhänsli et al. (1988), Finger and Steyrer (1990), Schaltegger et al. (1991), and von Raumer et al. (1999).

In the study area the Aar massif consists of pre-Variscan basement rocks with a polycyclic history and of Variscan plutonic rocks intruding the basement during the late Carboniferous and early Permian (Schaltegger 1993). The Variscan intrusives can be assigned to different magmatic suites (Schaltegger 1994). The 334 ± 2.5 Ma old (Schaltegger and Corfu 1992) Giuv syenite crops out at the surface along tunnel section but it is not present in the tunnel. The main pluton of the calc-alkaline central Aar granite (cAgr) intruded at 297 ± 2 Ma very close to the Carboniferous–Permian boundary. A sequence of volcaniclastic rocks (Fig. 1) including ignimbritic rhyolites and pyroclastic tuffs was deposited in the late Carboniferous to early Permian. The metarhyolites form the Windgällen formation in the north and the Tscharren formation south of Bristen (Oberhänsli et al. 1988). During Tertiary Alpine orogeny all rock units in the Gotthard section across the Aar massif were metamorphosed under greenschist facies conditions with increasing metamorphic grade from north to south (Frey et al. 1980). The position of the Bristen granite is just south of the high-grade side of the kaolinite–pyrophyllite reaction isograd (Frey 1987) corresponding to a temperature of about 300 °C for the Alpine metamorphic overprint. The Alpine assemblage of sheet silicates muscovite–chlorite–stilpnomelane–pyrophyllite (Breitschmid 1982) is present in appropriate rocks at the location of Bristen granite. The assemblage is characteristic for lower greenschist facies conditions.

The Brgr is part of the eastern Aar Massif, where three magmatic pulses are known (e.g., Schaltegger and Corfu 1995; Berger et al. 2017) with ages of 346–331, 315–307 and 299–295 Ma. The two older pulses belong to a shoshonitic-ultrapotassic series comprising diorites

shoshonitic-ultrapotassic series comprises diorites, syenites, and granites and a K-rich calc-alkaline series consisting of diorites and granites. Both series derive from an enriched mantle source high in Rb, K and Th. Both series can be related to similar sources in the subcontinental mantle and intruded the continental basement during an Andean-type subduction process (Schaltegger et al. 1991). The high-K calc-alkaline series experienced extensive fractional crystallization and possibly contamination by crustal melts (Schaltegger et al. 1991). The central Aar granite and the southern Aar granite represent intrusions tapped from late-orogenic deep crustal magma chambers during late Variscan strike-slip tectonics forming pull-apart basins (Schaltegger et al. 1991).

The Bristen granite has sharply discordant intrusive contacts to the granitic Erstfeld Gneiss in the North and to the pre-Variscan basement gneisses in the South (Fig. 2).

4 Samples, analytical methods and source of data

Four samples of Bristen granite from Tm between 8.438 and 8.868 km (Fig. 2), one sample each from the metarhyolites of the Intschi formation (Tm 10.035) and Tscharren formation (Tm 13.800) respectively, and two samples from the pre-Variscan basement (northern Schollen Zone, Tm 15.136) have been provided by NEAT in Amsteg during construction of the tunnel. Additional, samples of Bristen granite (five samples Tm 8.544–8.868) and central Aar granite (cAgr) (Tm 14.600) and southern Aar granite (sAgr) (Strem granite, respectively) (Tm 16.650) have been supplied by the Swiss Federal Office of Topography (Swisstopo) from their store of drill cores from the NEAT Gotthard rail base tunnel.

Whole rock analysis of these samples was performed by standard X-ray fluorescence (XRF) techniques at the University of Freiburg, Germany, using a Philips PW 2404 spectrometer. Fused beads were used for major elements, and powder pellets for trace elements. Relative standard deviations are < 1 and < 4% for major elements, respectively. Loss on ignition (LOI) was determined by heating at 1100 °C for 2 h. Rare earth elements (REE) and trace element analysis were performed by sodium peroxide fusion ICP AES at SGS Minerals Services in Lakefield, Ontario Canada. Bristen granite contains a maximum of 0.15% F based on the amout of fluorite and F-bearing mica present.

Mineral composition data were produced with a Cameca SX-100 electron beam micro analyzer (EPMA) at the University of Freiburg. Analyzed major elements: Si, Ti, Al, Fe, Mn, Mg, Ca, Na, K, and F. Analyzed trace elements: Nb, Ta, Th, U, Pb, Y, La, Ce, Pr, Nd, Sm, Gd, Dy, Er, and Yb. All silicate minerals except plagioclase were measured with 15 kV acceleration voltage and a beam current of 20 nA. The beam current for plagioclase was 10 nA. Fluorite and the associated rare earth element (REE) carbonates were measured with two conditions: Ca, Sr and F were measured corresponding to the silicate minerals but yttrium and the REEs were analyzed with a beam current of 100 nA. Niobates, thorite, and heavy REE were measured with 25 kV acceleration voltage and a beam current of 20 nA.

Kα-lines were used for major element analysis. Lines used for REE, Y, Pb, Th and U analyses were: $L\alpha_1$ (LIF) for La, Ce, Y; $L\beta_1$ (LIF) for Nd, Sm, Pr, Gd, Dy, Er, Yb; α_1 (PET) for Th; $M\beta_1$ (PET) for Pb, U. Raw data were corrected using the PAP method (Pouchou and Pichoir 1984). Relative errors for REE, Y are dependent on absolute abundances of each element and are estimates at < 1% at the > 10 wt% level; between 5–10% at the 1 wt% level and ~ 30% at the < 0.1 wt% level. Analytical precision for low concentrations (i.e. < 0.1 wt%) of U, Th and Pb is higher at ~ 10%. For single spot analyses detection limits for REE's and Y are approximately 150–400 ppm; U, Th and Pb are ~ 100 ppm. Elements analyzed but not listed in the Tables have been below detection limit. The Kα line of F has been analyzed using a PC0 crystal. The concentration of F can be empirically corrected for the major interference of Ce $L\alpha_1$ on F Kα (Förster 2001). Y and REE elements have been calibrated using phosphate standards, Nb and Th using oxide standards.

5 Petrographic description of Bristen granite

Bristen granite is a leucocratic rock with less than 5 vol.% mafic minerals (Fig. 3). The fine-grained rock is equigranular with grain sizes varying between 0.5 mm and 3 mm. The compact granite is very homogeneous along the outcrop in the tunnel and shows no foliation. The granite consists mainly of quartz (~ 35 vol.%), alkali-feldspar (~ 40 vol.%), plagioclase (~ 20 vol.%), and biotite (< 5 vol.%). Quartz appears predominantly as anhedral crystals up to 3 mm in size. Quartz is slightly deformed and shows beginning recrystallization in the very south of the stock (Fig. 4a). Fluid inclusions are present locally. K-feldspar is of the same grain size as quartz; in some samples larger Kfs porphyroblasts are present (Fig. 4) (all abbreviations of mineral names after Whitney and Evans, 2010). Most grains show coarse perthitic exsolutions as strings, rods and patches (Figs. 4b and 4c). Very coarse albite exsolution patches in large Kfs are in optical continuity (Fig. 4b). Some larger Kfs grains show textures suggesting a two-stage exsolution history (Fig. 4c). Albite (plagioclase) in the matrix occurs mostly as smaller grains (0.5–1 mm) and its mode is about half of that of Kfs. The textures indicate

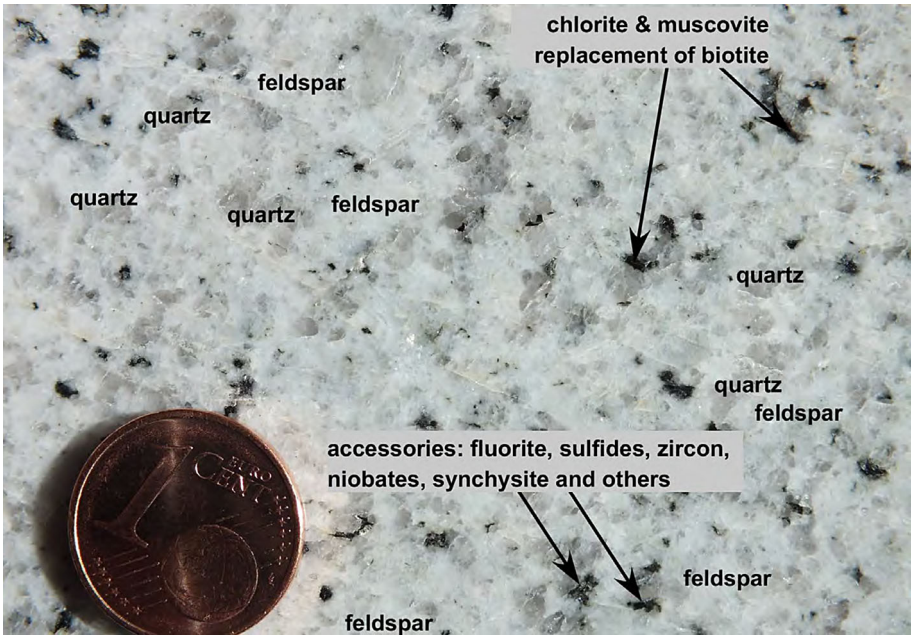

Fig. 3 Bristen granite, polished rock surface. Diameter of 1 cent (Euro) coin = 16 10^{-3} m

that albite is not a solidus mineral but formed from subsolidus decomposition of ternary alkali-feldspar (mesoperthite). The Qtz-Fsp matrix is fractured and different generations of veins with characteristic assemblages are present. Albite–chlorite veins represent the earliest generation (Fig. 4d).

Mafic minerals include chlorite, muscovite and biotite. Chlorite replaces primary igneous brown biotite and it occurs also in veins together with albite (Figs. 4d and 6a). Muscovite is typically associated with biotite and chlorite (Figs. 5a and 5b). It also occurs as vein filling mineral along micro-fractures (Figs. 4b, 4c and 5c). The textures suggest that muscovite does not occur as primary solidus mineral. Biotite is the major mafic solidus phase. It is always fine grained (0.5 and 1.5, up to 3 mm in the south) and partly or completely altered (Figs. 5a, b, d and 6a). The alteration products are chlorite, muscovite and various opaques (Fig. 6a and text below). No epidote or titanite is part of the alteration product assemblage. Stilpnomelane grows from primary biotite together with chlorite (Fig. 5d).

Accessory minerals found in the Bristen granite include fluorite, calcite, zircon, synchysite, parisite, Ti-niobates, REE-niobates, thorite, ilmenite, magnetite, pyrite, pyrrhotite, sphalerite, galena and other opaques. Fluorite occurs either as rather euhedral crystals (Figs. 7a, b) anhedral crystals (up to 0.75 mm in diameter) in the matrix of the rock or in micro-fractures. REE- and Y-rich fluorite overgrows primary igneous fluorite with which it is complexly intergrown.

Calcite ($\sim$ 0.1 mm) overgrows other minerals, mostly feldspars. Calcite is also present in micro-fractures (Figs. 4b and 5c) and small veinlets (Fig. 4c). Calcite is typically associated with other carbonates (e.g. synchysite) and accessory minerals in intensely fractured portions of the rock (Fig. 5c). Synchysite occurs as inclusions in fluorite (Figs. 7a, c). However, in some textures synchysite overgrows Y-fluorite (Fig. 7b).

Rare subhedral titanite (0.1–1 mm) is associated with mica (muscovite). Opaque minerals (ca. 0.5, 0.9 vol.% in the south) are mostly pyrite and pyrrhotite, but include also sphalerite and galena associated with titanite, fluorite and calcite. No apatite or other phosphates (e.g. monazite, xenotime) has been found in any of the samples. The very low concentration of P_2O_5 (< 0.01 wt%) in the rock (see section on rock composition) makes it unlikely that a phosphate grain, if any is present, is cut by a thin section. The rock contains abundant, up to 0.2 mm large euhedral zircon crystals dispersed in the rock matrix or as inclusions in biotite (Fig. 6a). Some of the rare accessory minerals are associated with zircon (see below).

The minerals typically occur as very small (5–20 μm) roundish grains that resemble droplets. These small beads are typically associated with chloritized biotite, sulfide aggregates or with zircon. Details on the textures will be presented in the mineral composition section below using Back Scatter Electron images (BSE) from the microprobe.

6 Composition of minerals

6.1 Silicate minerals

Plagioclase of Bristen granite is almost pure albite. Average anorthite component is $An_{2.6}$ with a variation

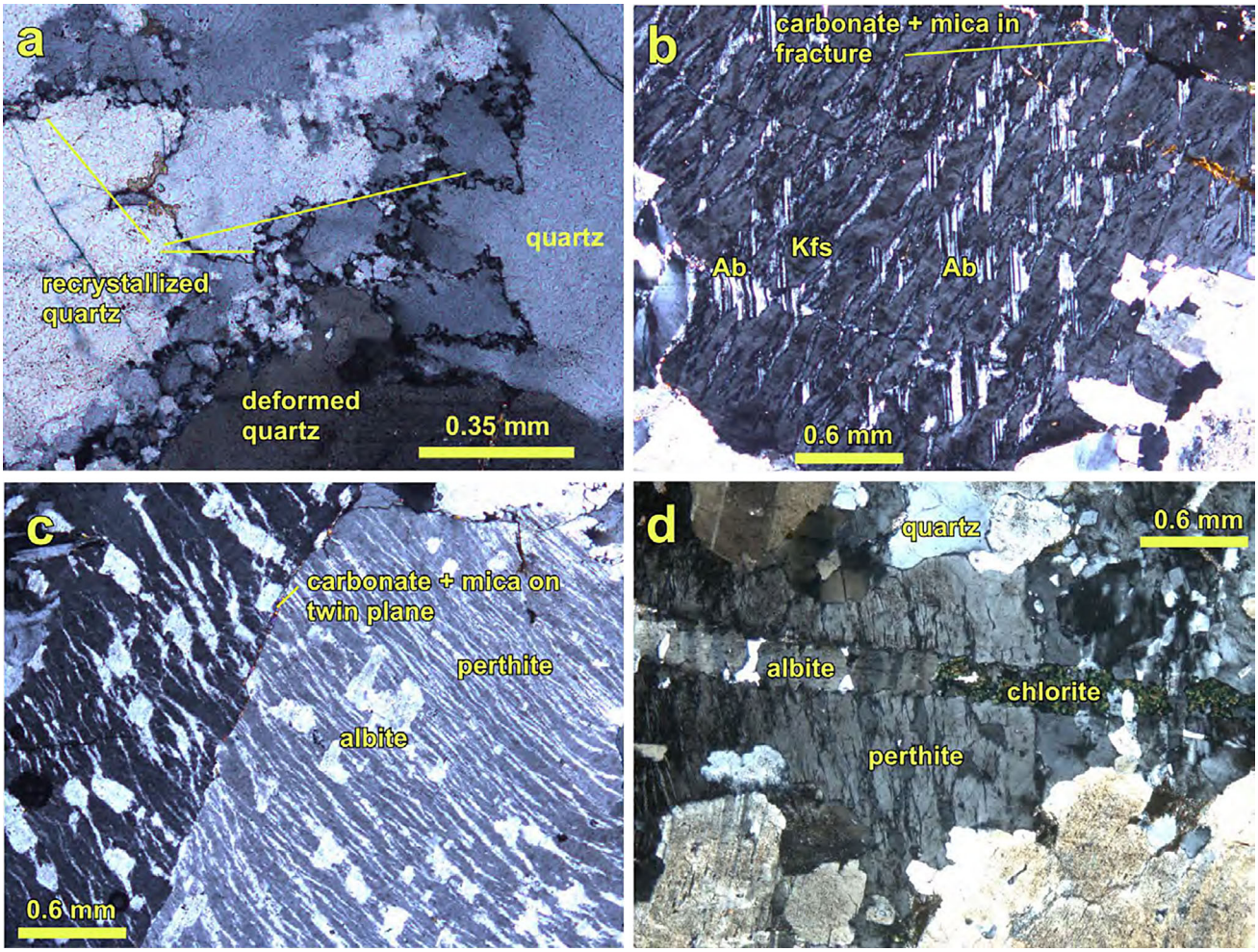

Fig. 4 Bristen granite (photomicrographs): **a** Deformed and recrystallized quartz, **b** Large alkali feldspar with coarse albite exsolution patches, calcite and mica in fractures, **c** Large twin of alkali feldspar (mesoperthite) with albite exsolution rods and patches, calcite and mica on twin plane, **d** Alkali feldspar (perthite) with vein sealed by albite and chlorite

from $An_{0.1}$ to $An_{5.0}$ (Table 1). Also Kfs (Or) in albite is extremely low and independent on texture. Matrix albite and albite exsolution patches (Figs. 4b and 4c) have the same composition. The composition of *K-feldspar* ranges from Ab_2 to Ab_9 (average Ab_4). Rubidium (up to 0.1 wt. % Rb_2O) is unusually high. Barium is absent, in sharp contrast to tunnel samples of the central Aar granite (Table 1). With the exception of Rb and Ba, feldspar composition in Brgr and cAgr are identical.

All sheet silicates of Brgr are characterized by very low magnesium. *Biotite* has an extremely high X_{Fe} of 0.95 and its composition is close to 50 mol % annite and 50 mol % ferro-eastonite. The average titanium content of biotite is 1.03 wt. %. Ti is higher than the average Mg concentration of 0.99 wt. % (Table 2) but low compared to biotite from cAgr from the tunnel (Table 2). Biotite contains fluorine (maximum: 0.59 wt. %, average: 0.45 wt. %). X_{Fe} of sheet silicates in cAgr is much lower than of those in Brgr (Table 2).

Conversion of biotite to *chlorite* and *muscovite* is common in all samples (Figs. 5a, b and 6a) and as a consequence of this conversion a wealth of opaque minerals formed as very small-grained byproducts (Fig. 6a). These byproducts include a multitude of REE-Y- and Nb-bearing minerals indicating that the primary igneous biotite contained these elements incorporated in its structure. These elements in biotite could not be analyzed by the microprobe (see Charoy and Raimbault 1994). The biotite transformation is often incomplete with intermediate stages preserved. Chlorite contains no titanium, potassium, and fluorine (Table 2). Like biotite, chlorite contains very little magnesium ($X_{Fe} = 0.96$). However, chlorite captures much of the manganese released by biotite alteration.

K-white mica is a muscovite with considerable Fe-tschermak component and can be termed phengite. The average FeO content of muscovite is 7.45 wt. % (Table 2). Magnesium is very low ($X_{Fe} = 0.88$). Muscovite contains

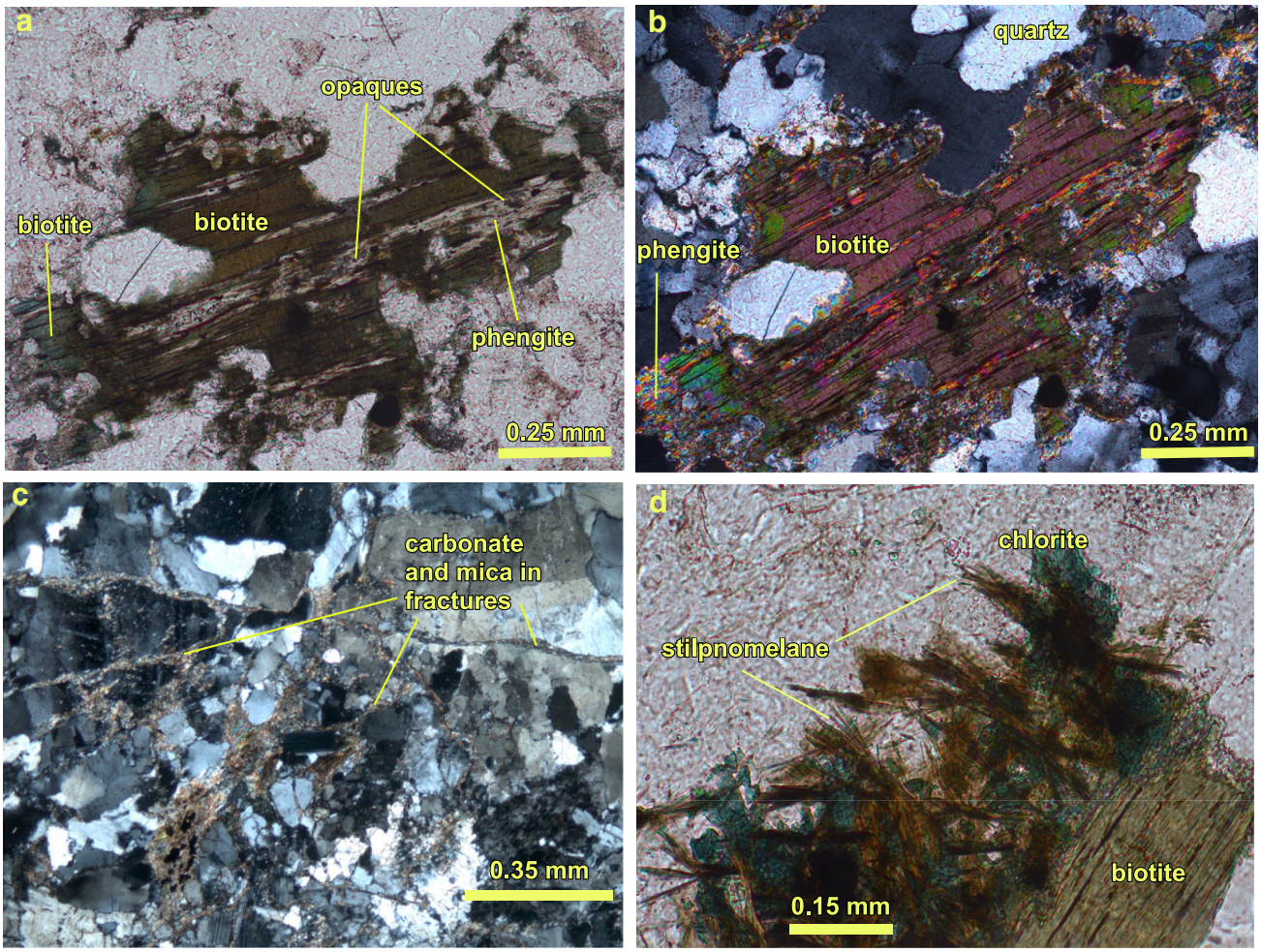

Fig. 5 Bristen granite photomicrographs: **a** Primary igneous biotite partly replaced by muscovite and opaques. Dark areas and black spots within the pseudomorph are additional replacement minerals, including ilmenite, magnetite, sulfides, various niobates, and others. **b** Same as **a** with crossed polars, **c** Fractured feldspar and quartz matrix with carbonate and accessory minerals in small fractures, **d** Primary igneous overgrown with chlorite and stilpnomelane

Rb up to 0.55 wt. % Rb_2O (average 0.25 wt. %) and up to 0.79 wt. % fluorine (average 0.55 wt. %).

Allanite is a very rare accessory silicate mineral in the Bristen granite. If present, it is partially replaced by epidote. The composition of preserved allanite is given in Table 3. It contains about 20 wt% yttrium and REE.

6.2 Fluorite, REE minerals and other accessories

Fluorite is an accessory matrix mineral forming small subhedral grains (Fig. 7a). Some fluorite can be found in micro fractures and veins. Its composition is similar to matrix fluorite. Fluorite is always intergrown with synchysite $Ca(REE,Y)(CO_3)_2F$, a Ca-carbonate mineral containing fluorine, yttrium and rare earth elements (Fig. 7a, b). Fluorite has an inhomogeneous composition with areas of stoichiometric CaF_2 and patchy regions rich in yttrium and also locally REE (Fig. 7c, Table 4). The predominant REE in fluorite are lanthanum (La), cerium (Ce) and neodymium (Nd). Fluorite occurring as cm-large euhedral crystals in open alpine fissures of the Aar massif has often a pink color, which is attributed to the presence of yttrium in the mineral (Armbruster et al. 1996).

Synchysite is an abundant accessory mineral in Bristen granite. It occurs in quite different textures: (a) It is often present as rims and inclusions of fluorite (Fig. 7), (b) The mineral occurs in clusters of fine-grained products of biotite decomposition together with sulphides, niobates and zircon, (c) Synchysite occurs also together with calcite in fractures and veins. The composition of synchysite ranges from Y-rich varieties to Ce-rich types (Table 5). Large calcite grains in veins may contain small inclusions of both Y-synchysite and Ce-synchysite. The total of REE varies considerably in synchysite (Table 5), however the Ce–La–Nd proportion remains constant (Fig. 8). The total of REE and Y is constant and the elements fill one site per formula

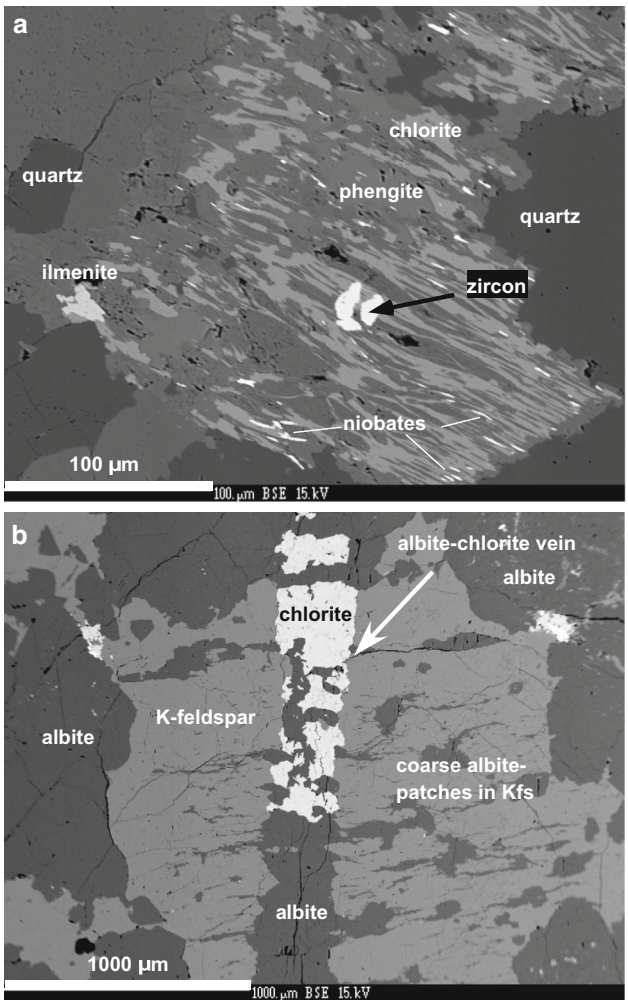

Fig. 6 BSE texture images, sample KB1349: **a** Biotite replaced by chlorite, muscovite, ilmenite and accessories including zircon and various niobates, **b** chlorite—albite vein (Fig. 4d) through coarse mesoperthite

unit (2.5 oxygen, ideal stoichiometry $Ca(Y,REE)(CO_3)_2F$. Synchysite contains predominantly light REE, heavy REE are at trace levels only. Rare parisite $Ca(Y,REE)_2(CO_3)_3F_2$ occurs occasionally intergrown with synchysite (Table 5).

Sulfides are typically associated with chloritized biotite seen as dark patches on Fig. 3. Pyrite is the predominant sulfide (Fig. 9). Other sulfides present include pyrrhotite, arsenopyrite, sphalerite, galena, and chalcopyrite. Pyrite locally contains abundant small (5–30 µm) inclusions of Y–Ti niobates, zircon and ilmenite (Fig. 9). The minerals replace biotite, together with chlorite and muscovite.

Ilmenite is abundant and forms nuggets of opaques, often together with sulfide, as a byproduct of biotite chloritization. ***Magnetite*** is typically related to Chl-Ph pseudomorphs after biotite. The mineral is rich in Mn and associated with ilmenite and occasionally with REE-carbonate.

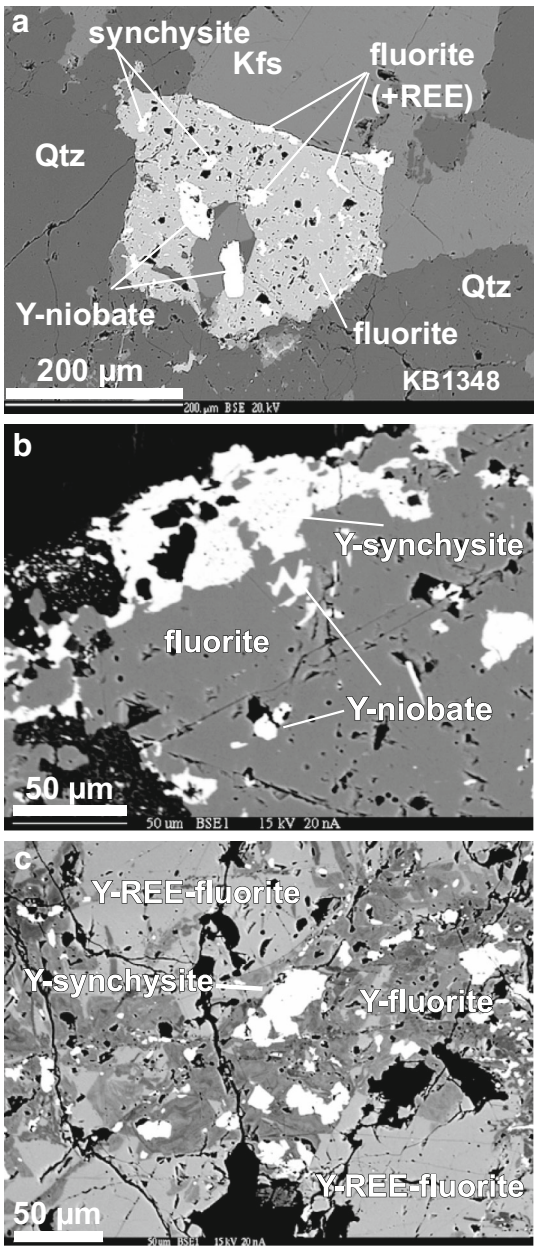

Fig. 7 BSE texture images of REE-minerals and fluorite in sample KB1348: **a** fluorite associated with Y-synchysite and CeYNdLa-synchysite and **b** Y-fluorite and Y-REE-fluorite intergrown with Y-synchysite

Zircon occurs both as perfectly euhedral small crystals (50-300 µm) in the patches of chloritized biotite and as irregular shaped grains in the feldspar-quartz matrix. Zircon contains abundant small inclusions of *thorite* ($ThSiO_4$) (5–20 µm). Thorite contains about 30 mol % coffinite ($USiO_4$) (Table 6). The totals of thorite suggest that the metamict phase did not take up water because it occurs as inclusions in zircon. Zircon also contains small inclusions of an Y-silicate, presumably yttrialite $(Y,Th,U)_2Si_2O_7$, a mineral of the thortveitite group. Also yttrocolumbite

Table 1 Feldspar composition

Feldspar	Plag	Plag	Plag	Kfs	Kfs	Plag	Kfs
Geol. unit	Brgr	Brgr	Brgr	Brgr	Brgr	cAgr	cAgr
# Points	11	1	1	24	1	9	7
SiO_2	68.45	68.57	67.85	64.45	64.78	68.49	63.43
Al_2O_3	20.02	19.86	20.39	18.28	18.2	20.23	18.8
FeO	0.07	0.07	bd	0.07	0.11	0.03	0.06
CaO	0.56	0.02	0.94	0.01	0.03	0.67	2.14
Na_2O	11.46	11.61	10.64	0.44	0.6	11.52	0.57
K_2O	0.13	0.13	0.15	15.97	16.58	0.08	15.07
Total	100.72	100.27	100	99.24[a]	100.31[a]	101.03	100.08[b]
Oxygen	8	8	8	8	8	8	8
Si	2.974	2.987	2.964	2.999	2.995	2.967	2.968
Al	1.025	1.019	1.050	1.003	0.992	1.033	1.037
Fe(2)	0.003	0.003	–	0.003	0.004	0.001	0.002
Ca	0.026	0.001	0.044	0.000	0.001	0.031	0.001
Na	0.965	0.980	0.901	0.040	0.054	0.967	0.051
K	0.007	0.007	0.008	0.948	0.978	0.004	0.959
An	2.61	0.09	4.61	0.05	0.14	3.10	0.10
Ab	96.67	99.17	94.51	4.02	5.21	96.46	5.11
Or	0.72	0.73	0.88	95.93	94.65	0.44	94.79

[a]Total includes 0.1 wt % Rb_2O

[b]Total includes 2.14 wt% BaO; TiO_2, MnO and MgO below detection limit (bd) of ~ 0.05 wt%

((Y,U,Fe)(Nb,Ta)O_4) is occasionally present (Table 7). Moreover, zircon frequently contains small inclusions of fergusonite ($YNbO_4$). Irregular-shaped grains of zircons near chlorite pseudomorphs after biotite are frequently mantled with ilmenite and associated with Mn-rich magnetite.

Niobates are widespread in the Bristen granite and occur as very small roundish droplet-shaped 5–20 µm sized grains. Most commonly niobates occur in chlorite–muscovite pseudomorphs after biotite together with sulfides, ilmenite, zircon and other accessories (Figs. 6a and 9). Niobates occur also as inclusions in zircon. Several types of niobates are present. However, the assignment of the analyses to specific minerals is difficult because many of the analyses contain components from the matrix surrounding the very small niobate grains. The tiny niobate grains are probably all metamict due to the high content of Th and U in these minerals, now glasses. Furthermore, the totals of the analyses are typically low because of uptake of secondary water during metamictization. Nevertheless, there are three major types of niobates present: a) Y-REE-niobate close to fergusonite stoichiometry (Table 8). It occurs, for example, in groups of small elongated grains overgrown by ilmenite in Bt-Chl-Ph spots, b) at least four different species of Y–Ti-REE-niobates. The analyses suggest the presence of aeschynite ((Y,REE,Ca)(Ti,Nb)$_2$(O,OH)$_6$) and polycrase ((Y,REE,U,Th)(Ti,Nb,Ta)$_2O_6$) (Hanson et al. 1992), other possible Ti-niobates include euxenite ((Y,Ca,Ce,U,Th)(Nb,Ta,Ti)$_2O_6$) (Duran et al. 2016) and samarskite ((Y,REE,U)$_3$(Nb,Ta,Ti)$_5O_{16}$). However, the proposed reaction model for aeschynite and polycrase by Hanson et a. (1992) suggests crystallization from a P- and F-depleted residual melt. Partial analyses of two groups of Ti-niobates (Y-Nb titanates) are given in Table 9. The compositions have been normalized to 2 cations and 4 oxygens corresponding to the stoichiometry of fergusonite. The partially low totals may indicate that the phases contain some secondary water due to metamictization, c) U-Th-bearing niobate occurs associated with fergusonite, pyrite and coffinite.

7 The composition of Bristen granite

Bristen granite has an average SiO_2 content of 77.4 wt. % (Table 10) and is the most silica-rich granite of all Aar massif granites. It is a subalkaline granite with a weakly peraluminous character [$Al_2O_3/(CaO + Na_2O + K_2O) = 1.02$]. The small modal amount of mafic minerals is reflected in the low concentrations of FeO, MnO, MgO and TiO_2 (Table 11). The samples contain very little P_2O_5 (< 0.01 wt. %), which is in accordance with the absence of apatite and other phosphate minerals such as monazite or xenotime. Table 10 lists the major element composition of the samples of Bristen granite. The major element composition of samples from the central Aar granite, the

Table 2 Composition of sheet silicates, muscovite, biotite and chlorite

Mineral Geol. unit # Points Assemblage	Muscovite Brgr 16	Muscovite Brgr 1	Muscovite Brgr 1 ps	Muscovite cAgr 4	Biotite Brgr 15	Biotite cAgr 10	Chlorite Brgr 17 Matrix	Chlorite Brgr 1 ps	Chlorite Brgr 1 Chl-Ab vein	Chlorite cAgr 10
SiO_2	47.95	46.30	43.92	47.85	34.25	35.79	22.71	22.81	22.45	25.38
TiO_2	0.16	0.28	0.31	0.01	1.03	1.57	0.06	0.15	0.07	0.06
Al_2O_3	28.96	28.46	27.07	29.79	17.45	16.2	19.42	18.93	20.11	18.73
FeO	7.45	8.38	8.81	4.25	31.48	24.36	43.43	41.45	42.36	32.11
MnO	0.11	0.18	0.26	0.04	0.55	0.54	1.36	2.03	2.15	1.04
MgO	0.58	0.58	0.57	1.90	0.99	7.59	1.03	1.4	1.31	10.37
CaO	0.02	0.02	1.56	bd	0.04	0.06	0.04	0.08	0.04	0.07
Na_2O	0.10	0.08	0.11	0.18	0.09	0.06	0.04	0.03	bd	0.03
K_2O	10.27	10.94	10.66	10.83	8.71	9.08	0.07	0.09	0.01	0.03
F	0.55	0.45	0.41	0.11	0.45	0.34	bd	bd	bd	bd
Total[d]	94.74[a]	94.26	92.29	94.16[b]	93.82	94.48[c]	88.16	86.33	88.51	87.82
Oxygen	22	22	22	22	22	22	28	28	28	28
Si	6.543	6.429	6.308	6.503	5.585	5.598	5.344	5.415	5.247	5.583
Al(IV)	1.457	1.571	1.692	1.497	2.415	2.402	2.656	2.585	2.753	2.417
sum T	8.000	8.000	8.000	8.000	8.000	8.000	8.000	8.000	8.000	8.000
Ti	0.016	0.029	0.033	0.001	0.126	0.185	0.011	0.027	0.012	0.010
Al(VI)	3.200	3.086	2.890	3.274	0.938	0.584	2.732	2.711	2.788	2.440
Fe(II)	0.850	0.973	1.058	0.483	4.292	3.186	8.547	8.227	8.279	5.907
Mn	0.013	0.021	0.032	0.005	0.076	0.072	0.271	0.408	0.426	0.194
Mg	0.118	0.120	0.122	0.385	0.241	1.770	0.361	0.495	0.456	3.400
Ca	0.003	0.003	0.240	–	0.007	0.010	0.010	0.020	0.010	0.016
sum M	4.200	4.232	4.375	4.148	5.680	5.807	11.932	11.888	11.971	11.967
Na	0.026	0.022	0.031	0.047	0.028	0.018	0.018	0.014	–	0.013
K	1.788	1.938	1.953	1.877	1.812	1.812	0.021	0.027	0.000	0.008
sum I	1.814	1.960	1.984	1.924	1.840	1.830	0.039	0.041	0.000	0.021
F	0.237	0.198	0.186	0.047	0.232	0.168	–	–	–	–
X_{Fe}	0.88	0.89	0.90	0.56	0.95	0.64	0.96	0.94	0.95	0.63

ps Ms + Chl pseudomorph after Bt, *bd* below detection limit

Total includes: [a]0.25 Rb_2O; [b]0.52 BaO; [c]0.11 BaO; [d] correction for O=F,Cl; traces of Cl in micas; Ms contains 15, 21, 25, 27 Cel

southern Aar granite, the meta-rhyolites of the Intschi and Tscharren formation, respectively, and for comparison from the pre-Variscan gneisses can be found in Table 11.

The CIPW norm composition of Bristen granite contains an average of 97.5 vol.% quartz and feldspar corresponding to the same differentiation index of 97.5 (Hollocher 2007) (Aar granite: 94). There is about 0.7 vol.% of normative corundum (range: 0.2–1.2) underlining its peraluminous character. Normative hypersthene is below 1 vol.%, the total of normative ilmenite, magnetite and apatite is < 0.2 vol.%. There is about 0.3 vol.% normative fluorite in Bristen granite. The computed normative An and Ab combines to a plagioclase with a molar $X_{An} = 2.9$ compared to the measured average plagioclase $X_{An} = 2.6$ (Table 1). $X_{Mg} = 0.05$ is extremely low and underscores the highly differentiated character of Brgr (cAgr: $X_{Mg} \sim 0.4$). The estimated liquidus temperature is about 700 °C at an H_2O content of 4.9 wt%. The corresponding liquidus temperatures for cAgr and sAgr are 832 and 841 °C, respectively (following Hollocher 2007). The normative feldspar and quartz content of the Brgr (Fig. 10) corresponds to a feldspar composition of Kfs 44 – Pl 56, or a ternary feldspar composition of $Or_{44}Ab_{53}An_3$.

The concentration data for the oxides of Al, K, Na, and Ca of all analyzed samples cluster close to the 1–1 intersection on the ANKC diagram (Fig. 11). However, the data are well separated for the different rock types and the Brgr samples define a linear array in the field of peraluminous granites. The samples from central and southern Aare

Table 3 Allanite analyses

Point	43	31
SiO_2	33.51	33.71
TiO_2	0.44	0.27
Al_2O_3	15.46	15.19
Fe_2O_3	13.41	13.66
Y_2O_3	12.66	12.24
REE	8.43	9.55
FeO	0.45	0.51
MnO	1.46	1.54
CaO	12.19	11.40
F	0.11	0.20
H_2O	1.57	1.52
Total	99.70	99.79
O = F	0.05	0.08
Total	99.65	99.71
Si	3.003	3.032
Ti	0.030	0.018
Al^{3+}	1.633	1.610
Fe^{3+}	0.904	0.925
Mn^{2+}	0.111	0.117
Ca^{2+}	1.170	1.099
Y^{3+}	0.604	0.586
REE^{3+}	0.269	0.307
F	0.031	0.057

Oxides in wt%, stoichiometry per 12.5 oxygens, with all Fe as Fe^{3+}

granite, respectively, are distinctly displaced relative to the Brgr samples because of higher Al in the Aare granites.

The Bristen granite data can be connected by linear arrays to the meta-rhyolites and the Aar granites on all Harker-type diagrams of Fig. 12 in contrast to the basement samples. All represented components decrease drastically with increasing SiO_2, except the total alkalis. The total alkalis remain constant at about 8 wt. %. The very low Fe, Ti, P and Ca of the Brgr together with the ultra-low Mg characterize the leucocratic granite.

The low FeO and CaO of Intschi and Tscharren metavolcanics (Table 11) suggests that they are derived from typical W-type rhyolites (Izett 1981) generated in regions underlain by granitic crust undergoing extension.

Rubidium Rb is with an average of about 400 ppm and a maximum of 500 ppm very high in Brgr (Table 12) whilst cAgr contains about 100 ppm Rb only (Fig. 13). Sr and Ba concentrations are very low (Ba from below detection limit to 30 ppm) (Table 12). Rb and Ba is negatively correlated and the average Brgr, sAgr and cAgr define a linear trend with $R^2 = 0.985$. Also Y and Nb are much higher in the Brgr compared with the Aar granites (Fig. 13).

Table 4 Composition of fluorite

#Points	Fluorite	Y- bearing fluorite	
	14	7	8
CaO[a]	71.45	67.43	65.36
Y_2O_3	0.15	4.36	4.84
La_2O_3	0.01	0.01	0.34
Ce_2O_3	0.02	0.02	1.21
Nd_2O_3	0.02	0.03	0.85
F	47.99	48.48	48.08
Total[b]	119.64	120.33	120.68
O=F	20.21	20.41	20.24
Total	99.44	99.92	100.43
Ca	0.998	0.954	0.931
Y	0.001	0.031	0.034
La			0.002
Ce			0.006
Nd			0.004
F	1.979	2.024	2.022
REE + Y	0.001	0.031	0.046

[a]Oxides in wt%

[b]Contains traces of Sr

The granite contains 0.14 wt. % fluorine resulting in 0.33 vol.% normative fluorite. The trace element pattern (Fig. 14) is characteristic of very highly differentiated and evolved granites (Jahn et al. 2001; Hollocher et al. 2016). It shows very low Ba, Sr, Eu and Ti compared to Aar granite. In contrast, Th, U, Nb and Y are much higher in Brgr compared to Aar granite.

Total of REE is about 150 ppm, lower than in the cAgr ($\sim$ 250 ppm) (Table 13). However, the Bristen granite contains drastically more heavy REE (Tb to Lu) than Aar granite (Table 13). The wt% portion of HREE is eight times higher in Brgr than in cAgr (Fig. 15). The chondrite normalized REE patterns of all Brgr samples are very similar showing a very low Eu point in otherwise flat patterns (Fig. 16) very similar to other highly evolved granites (Jahn et al. 2001). The patterns are in sharp contrast to the patterns of Aar granite showing a general decrease of REE with increasing atomic number and no Eu anomaly. In the HREE pattern of Brgr the lanthandide tetrad effect is evident (Irber 1999; Jahn et al. 2001; Monecke et al. 2002).

8 Alpine fissure minerals

In contrast to the rocks, particularly granite, further south in the Amsteg section of the NEAT tunnel where spectacular alpine fissure minerals are common, few

Table 5 REE carbonates synchisite and parisite. Synchisite analyses arranged with decreasing Y content

Mineral	Synchisite-Y									Synchisite-Ce		Parisite		
Point	4	12#	14	7	5	6	7	8#	33	27	8	4	4#	3
Y_2O_3	18.89	18.53	17.76	17.35	15.04	13.05	12.45	11.38	10.89	10.88	2.69	3.95	4.66	4.92
La_2O_3	3.56	3.51	3.71	3.78	3.82	5.69	5.40	5.82	5.21	4.77	6.76	9.10	8.40	8.79
Ce_2O_3	9.99	10.17	10.19	9.95	10.52	12.72	14.19	15.44	14.86	14.54	20.44	24.75	22.34	22.32
Pr_2O_3	1.38	1.02	1.43	1.61	1.23	1.76	1.27	1.60	2.09	2.22	2.85	2.88	2.73	2.76
Nd_2O_3	5.97	6.93	6.71	6.70	6.28	7.62	7.49	8.49	8.97	9.08	11.28	11.41	10.27	10.45
Sm_2O_3	2.20	1.60	2.17	2.46	2.31	2.14	2.18	2.10	3.03	3.13	3.53	2.67	2.52	2.42
Gd_2O_3	3.35	2.43	3.59	3.27	3.57	2.43	2.22	2.32	3.18	3.61	3.01	2.04	2.41	2.67
Dy_2O_3	2.47	1.32	2.02	2.16	2.53	1.55	1.18	2.22	1.12	1.93	0.48	0.45	0.52	0.43
CaO	19.50	17.47	19.08	19.88	19.66	18.64	18.04	16.18	19.31	19.20	18.76	10.51	10.22	10.91
F	6.21	5.84	6.34	6.29	5.97	5.95	5.99	5.78	6.20	6.17	6.12	6.83	6.62	6.52
Total[a]	73.52	68.82	73.00	73.45	70.93	71.57	70.42	71.34	74.86	75.53	75.92	75.45	71.77	72.75
O=F	2.61	2.46	2.67	2.65	2.51	2.51	2.52	2.43	2.61	2.60	2.58	2.88	2.79	2.75
Total corr.	70.91	66.36	70.33	70.80	68.42	69.06	67.90	68.90	72.25	72.93	73.34	72.57	68.98	70.00
CO_2 stoich wt	30.19	28.00	29.66	30.16	29.16	28.63	27.95	27.12	29.50	29.59	28.53	24.44	23.52	24.01
Total incl CO_2	101.23	94.47	100.02	101.05	97.70	97.80	95.86	96.09	101.81	102.61	101.87	97.08	92.53	94.16
Y	0.489	0.514	0.468	0.452	0.407	0.357	0.348	0.323	0.289	0.288	0.074	0.191	0.235	0.243
La	0.064	0.067	0.068	0.068	0.072	0.108	0.105	0.114	0.096	0.087	0.129	0.305	0.293	0.301
Ce	0.178	0.194	0.185	0.178	0.196	0.239	0.273	0.302	0.272	0.265	0.387	0.823	0.775	0.758
Pr	0.024	0.019	0.026	0.029	0.023	0.033	0.024	0.031	0.038	0.040	0.054	0.095	0.094	0.093
Nd	0.104	0.129	0.119	0.117	0.114	0.140	0.141	0.162	0.160	0.161	0.208	0.370	0.347	0.346
Sm	0.037	0.029	0.037	0.041	0.040	0.038	0.039	0.039	0.052	0.054	0.063	0.084	0.082	0.077
Gd	0.054	0.042	0.059	0.053	0.060	0.041	0.039	0.041	0.053	0.059	0.052	0.061	0.076	0.082
Dy	0.039	0.022	0.032	0.034	0.041	0.026	0.020	0.038	0.018	0.031	0.008	0.013	0.016	0.013
Fe	0.000	0.000	0.000	0.000	0.000	0.001	0.000	0.001	0.000	0.000	0.000	0.065	0.086	0.043
Ca	1.017	0.975	1.011	1.042	1.071	1.026	1.016	0.925	1.033	1.022	1.039	1.022	1.037	1.085
F	0.956	0.962	0.992	0.973	0.960	0.967	0.996	0.975	0.979	0.970	1.000	1.961	1.984	1.914
Ca	1.017	0.975	1.011	1.042	1.071	1.026	1.016	0.925	1.033	1.022	1.039	1.022	1.037	1.085
Y	0.489	0.514	0.468	0.452	0.407	0.357	0.348	0.323	0.289	0.288	0.074	0.074	0.074	0.074
REE	0.500	0.503	0.525	0.521	0.546	0.625	0.641	0.727	0.688	0.697	0.900	1.751	1.683	1.671
REE total + Y	0.989	1.016	0.992	0.972	0.953	0.982	0.989	1.050	0.978	0.985	0.974	1.825	1.757	1.745
Y/Ce	2.75	2.65	2.53	2.53	2.08	1.49	1.28	1.07	1.07	1.09	0.19	0.23	0.30	0.32

[a]Total includes traces of Fe, Sr

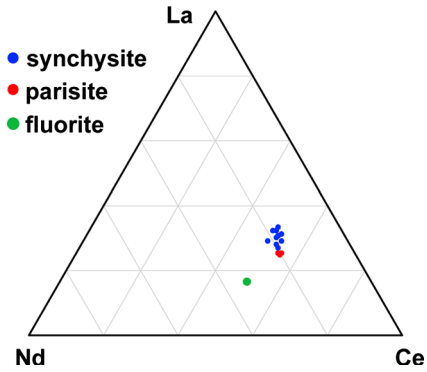

Fig. 8 REE in synchysite, parisite and fluorite: Ce–La–Nd in mole %

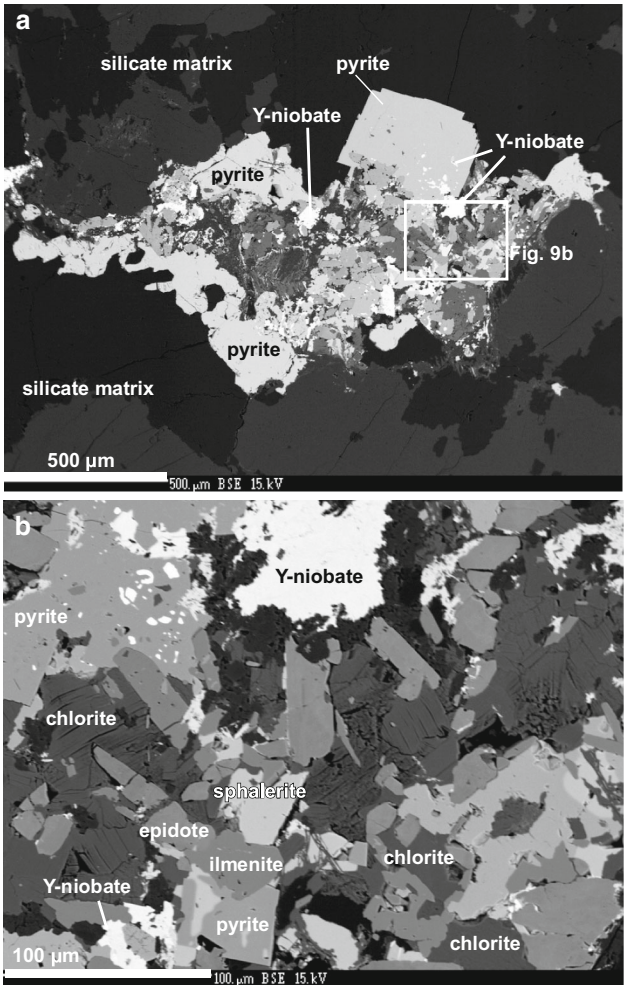

Fig. 9 BSE texture images of sulfides and niobates, sample KB1349: **a** Cluster of fine-grained minerals including pyrite, Y-niobates and Y–Ti–niobates in quartz-feldspar matrix, **b** Detail of white framed area on a) with niobates, sphalerite, pyrite, ilmenite, epidote and chlorite

mineralized fissures were opened in the Bristen granite. Rock crystal (quartz), anatase, and synchysite were found (Amacher and Schüppach 2011). In 1995, Swiss Rail rebuilt the hydroelectric power station in Amsteg. One of

Table 6 Composition of thorite

Mineral Point	Thorite 29	Thorite 30
SiO_2	18.61	19.36
ThO_2	52.72	52.30
UO_2	23.00	24.68
Y_2O_3	1.47	1.65
FeO	0.37	0.43
Total	96.33	98.57
Si	1.018	1.028
Th	0.656	0.632
U	0.280	0.292
Y	0.043	0.047
Fe	0.017	0.019
Sum M	0.996	0.989

[a]Oxides in wt%, stoichiometry per 4 oxygens

Table 7 Yttrocolumbite

Nb_2O_5	35.4	Nb	0.884
Ta_2O_5	5.8	Ta	0.084
ThO_2	1.8	Sum A	0.968
UO_2	31.6	Th	0.022
Y_2O_3	6.5	U	0.375
Nd_2O_3	0.2	Y	0.184
Sm_2O_3	0.1	Nd	0.004
Gd_2O_3	0.8	Sm	0.003
Dy_2O_3	0.8	Gd	0.014
Er_2O_3	2.7	Dy	0.014
Yb_2O_3	2.8	Er	0.044
FeO	5.7	Yb	0.045
CaO	1.2	Fe2	0.253
		Ca	0.071
Total	95.4	Sum B	1.030
		Total cations	1.997

La,Ca, Pr in traces, ideal cations = 2; ideal oxygens = 4

the new water tunnels ("Unterwasserkanal") closely approached, but did not intersect the Bristen granite. Euhedral minerals found in open Alpine fissures in mica-schist in this water tunnel included: Quartz, albite, calcite, chlorite, brookite, anatase, sphalerite, chalcopyrite, and pyrrhotite (Amacher and Schüppach 2011). REE-bearing minerals were found in the fissures of schists close to the Bristen granite including: Synchysite, monazite, and an unidentified mineral containing U and heavy REE (location U7 in Amacher and Schüppach 2011). Synchysite has also been reported from fissures of the cable and access tunnels connecting to the main rail tunnel (Amacher and Schüppach 2011).

Table 8 Composition of fergusonite (sample 1348)

Point	16	17	34	35
Nb_2O_5	42.63	40.19	41.09	41.94
Ta_2O_5	0.95	0.82	0.88	0.65
TiO_2	0.54	0.41	0.30	0.48
ThO_2	2.14	2.10	2.27	2.20
UO2	5.93	6.21	5.85	6.40
Y_2O_3	17.94	18.27	21.03	18.29
La_2O_3	0.01	0.02		
Ce_2O_3	0.15	0.22	0.07	0.24
Pr_2O_3	0.11	0.14	0.19	0.05
Nd_2O_3	1.81	1.87	1.51	1.35
Sm_2O_3	1.17	1.11	1.41	0.99
Gd_2O_3	3.28	3.49	3.80	3.10
Dy_2O_3	4.32	4.29	4.50	3.77
Er_2O_3	3.75	3.95	3.63	3.33
Yb_2O_3	3.55	3.69	3.48	3.57
FeO	1.79	1.26	0.87	1.71
CaO	0.96	0.98	0.99	0.99
Total	91.06	88.91	91.89	89.10
Nb	0.986	0.967	0.956	0.991
Ta	0.013	0.011	0.012	0.009
Ti	0.020	0.016	0.011	0.018
Th	0.024	0.025	0.026	0.025
U	0.065	0.071	0.065	0.072
Y	0.472	0.500	0.557	0.492
La	0.000	0.000	0.000	0.000
Ce	0.003	0.004	0.001	0.004
Pr	0.002	0.003	0.003	0.001
Nd	0.032	0.034	0.027	0.024
Sm	0.020	0.020	0.024	0.017
Gd	0.054	0.060	0.063	0.052
Dy	0.069	0.071	0.072	0.061
Er	0.058	0.064	0.057	0.053
Yb	0.054	0.058	0.053	0.055
Fe	0.074	0.054	0.036	0.072
Ca	0.051	0.054	0.053	0.054
sum	2.047	2.058	2.017	2.003
Nb + Ta	1.006	0.979	0.969	1.002
Cat–Nb–Ta	0.903	0.963	1.000	0.910

Oxides in wt%, stoichiometry per 4 oxygens, with all Fe as Fe^{2+}

9 Discussion

9.1 The Bristen granite in the framework of Variscan intrusives

The compositional features of Bristen granite (Figs. 11, 12, 13, 14, 15, 16, 17) are characteristic of reduced A-type granites, whilst the cAgr classifies as a normal calc-alkaline granite (e.g. Charoy and Raimbault 1994; Smith et al. 1999; Jahn et al. 2001; Wang et al. 2001; Anderson et al. 2003; Bucher and Frost 2006; Dall'Agnol and Oliveira 2007). A-type or highly fractionated granites with high LILE and HFSE abundances as well as pronounced negative anomalies (Sr, Eu, Ba, Ti) may result from extended fractional crystallization (e.g., plagioclase, ilmenite) (Smith et al. 1999; Anderson et al. 2003) or from melting of high-grade crustal rocks (Bartoli et al. 2016).

The Bristen granite is likely a late Variscan intrusion, suggested by the geological context of its occurrence in the Aar massif basement (Fig. 2). It can be regarded as a young member of the many Variscan granitoid intrusions elsewhere in the Aar massif, specifically of the Haslital intrusions as defined by Schaltegger (1994). Alternatively, Bristen granite could represent a separate isolated small stock genetically unrelated to the other Variscan granitoid intrusions. The very distinct trace element and REE patterns of the Brgr (Figs. 13, 14 and 16) could be the result of an origin independent from the central Aar granite.

However, leucocratic fine-grained granitoid bodies or units that resemble the Bristen granite have been reported from elsewhere in the Aar massif. A 200 m thick slab of strongly gneissose Aar granite known as northern border facies (nbf, Fig. 1) occurs 2.3 km south of the Brgr (Labhart 1977; Schaltegger and Corfu 1992, 1995). This leucocratic granite is similar to the Bristen granite in major element composition but it is strongly deformed in contrast to the Brgr. Also the garnet-bearing peraluminous Kessiturm aplite from the Grimsel area described by Stalder (1964) seems to have some similarities to the Bristen granite. The Mittagflue granite of the Haslital intrusions as defined by Schaltegger (1994) has mineralogical and geochemical properties similar to Bristen granite. It is a peraluminous fluorite- and garnet-bearing leucogranite with low Mg, Ti, and P and high Si (Schaltegger 1990). Bristen granite is slightly more evolved than Mittagflue granite though.

A possible co-magmatic relationship of Bristen granite with other Aar massif intrusions can be deduced from linear SiO_2 versus major element relationships of the rock composition data reported here and the averaged data of different granitoids from the Aar massif from Schaltegger (1990) including the Mittagflue leucogranite, the Kessiturm aplite, the leucocratic northern border facies of the cAgr and others (Fig. 1). The Brgr shows the most extreme position along these linear trends with the highest SiO_2, the lowest MgO, FeO, Ti and P of all intrusives of the Aar massif. However, these linear trends cannot be regarded as a prove that Brgr is co-magmatic with the other Aar massif granites. It simply shows that with increasing SiO_2 the rocks contain increasing modal feldspar at the expense of

Table 9 Partial analyses of two different Ti–Y-niobates (2 cations and 4 oxygens)

Point	20	22	19	2	11	12	16	17
TiO_2	43.60	43.76	41.55	28.81	28.66	26.96	26.32	25.67
Nb_2O_5	8.82	8.48	10.87	17.69	21.70	23.38	24.22	24.11
Ta_2O_5	0.32	0.31	0.36	0.92	1.50	1.33	1.45	1.34
ThO_2	0.19	0.33	0.36	0.81	0.99	1.93	2.35	2.28
UO_2	2.07	2.79	3.23	22.24	8.72	9.61	10.01	10.54
Y_2O_3	21.74	24.10	20.94	12.33	13.68	12.21	13.08	12.80
La_2O_3	0.03	0.13	0.11	0.00	0.02	0.09	0.00	0.03
Ce_2O_3	0.29	0.56	0.02	0.47	0.40	0.43	0.63	0.31
Pr_2O_3	0.18	0.29	0.07	0.03	0.11	0.02	0.00	0.14
Nd_2O_3	1.08	1.42	0.58	0.14	0.66	0.55	0.50	0.73
Sm_2O_3	0.76	1.01	0.53	0.42	0.63	0.36	0.68	0.87
Gd_2O_3	2.44	2.31	2.39	1.51	2.76	1.97	2.46	2.45
Dy_2O_3	2.66	3.54	3.59	2.18	4.48	4.10	3.62	4.04
Er_2O_3	3.94	4.58	3.58	3.99	5.12	5.18	5.08	6.00
Yb_2O_3	4.68	3.82	4.12	4.07	3.76	4.15	4.29	4.75
CaO	0.71	0.56	0.71	1.60	2.04	2.72	2.49	2.49
Total	93.50	97.99	93.00	97.22	95.22	94.99	97.19	98.55
Ti	1.911	1.867	1.843	1.404	1.353	1.285	1.239	1.212
Nb	0.240	0.225	0.300	0.536	0.637	0.693	0.710	0.708
Ta	0.005	0.005	0.006	0.016	0.026	0.023	0.025	0.023
Th	0.003	0.004	0.005	0.012	0.014	0.028	0.034	0.033
U	0.027	0.035	0.042	0.321	0.122	0.136	0.139	0.147
Y	0.674	0.727	0.657	0.425	0.457	0.412	0.436	0.428
La	0.001	0.003	0.002	0.000	0.001	0.002	0.000	0.001
Ce	0.006	0.012	0.000	0.011	0.009	0.010	0.014	0.007
Pr	0.004	0.006	0.001	0.001	0.003	0.001	0.000	0.003
Nd	0.022	0.029	0.012	0.003	0.015	0.012	0.011	0.016
Sm	0.015	0.020	0.011	0.009	0.014	0.008	0.015	0.019
Gd	0.047	0.043	0.047	0.032	0.057	0.041	0.051	0.051
Dy	0.050	0.065	0.068	0.046	0.091	0.084	0.073	0.082
Er	0.072	0.082	0.066	0.081	0.101	0.103	0.100	0.118
Yb	0.083	0.066	0.074	0.080	0.072	0.080	0.082	0.091
Ca	0.044	0.034	0.045	0.111	0.137	0.184	0.167	0.167
REE	0.301	0.325	0.283	0.264	0.361	0.341	0.346	0.388
Y	0.674	0.727	0.657	0.425	0.457	0.412	0.436	0.428
Th	0.003	0.004	0.005	0.012	0.014	0.028	0.034	0.033
U	0.027	0.035	0.042	0.321	0.122	0.136	0.139	0.147
sum	1.004	1.092	0.987	1.022	0.954	0.916	0.955	0.995
Y	0.674	0.727	0.657	0.425	0.457	0.412	0.436	0.428
LREE	0.048	0.069	0.027	0.024	0.040	0.033	0.040	0.046
HREE	0.252	0.256	0.255	0.240	0.321	0.308	0.306	0.342
REE total + Y	0.975	1.052	0.940	0.689	0.818	0.753	0.782	0.815
Nb	0.240	0.225	0.300	0.536	0.637	0.693	0.710	0.708
Ta	0.005	0.005	0.006	0.016	0.026	0.023	0.025	0.023
Ti	1.911	1.867	1.843	1.404	1.353	1.285	1.239	1.212
sum	2.156	2.097	2.149	1.957	2.016	2.001	1.974	1.943

Table 10 Major element composition of Bristen granite (Brgr) (wt %)

Sample	KB 1348a	KB 1361	KB 1362	KB 1350	KB 1363	KB 1364	KB 1349	KB 1365	Average	Std.dev
Tunnel meter[a]	8.438	8.544	8.610	8.745	8.745	8.770	8.868	8.868		
SiO_2	77.43	77.23	78.16	77.21	77.76	77.10	77.1	76.96	77.37	0.38
TiO_2	0.03	0.04	0.04	0.03	0.04	0.04	0.03	0.05	0.04	0.01
Al_2O_3	12.45	12.56	12.01	12.51	12.21	12.59	12.03	12.58	12.37	0.23
FeO[b]	0.66	0.79	0.62	0.75	0.67	0.86	0.81	0.85	0.75	0.08
MnO	0.02	0.04	0.03	0.03	0.03	0.03	0.03	0.03	0.03	0.01
MgO	0.01	0.02	0.03	0.02	0.03	0.03	0.03	0.03	0.03	0.01
CaO	0.56	0.46	0.43	0.42	0.41	0.42	0.42	0.41	0.44	0.05
Na_2O	4.18	3.81	3.40	4.06	3.67	3.92	4.03	3.69	3.85	0.24
K_2O	4.22	4.15	4.41	4.58	4.37	4.27	4.34	4.62	4.37	0.15
P_2O_5	0.01	0.01	0.01	0.01	0.01	0.01	0.01	0.01	0.01	0.00
Total major	99.57	99.11	99.14	99.62	99.20	99.27	98.83	99.23	99.25	0.24
LOI	1.22	0.66	0.84	0.31	0.71	0.49	0.55	0.57	0.67	0.25
Total[c]	100.79	99.77	99.98	99.93	99.91	99.76	99.38	99.80	99.91	0.37
$Na_2O + K_2O$	8.40	7.96	7.81	8.64	8.04	8.19	8.37	8.31	8.22	0.25

LOI Loss on ignition

[a]Distance from north portal in kilometer

[b]Total iron is given as FeO

[c]Total does not include a maximum of 0.15% F

Table 11 Major element composition of central Aar granite (cAgr), southern Aar granite (sAgr), Permian rhyolites (Intschi formation, Tscharren formation) and pre-Variscan basement (wt%)

Unit	CAgr	SAgr	Intschi	Tscharren	Basement
Sample	KB 1366	KB 1367	KB 1356	KB 1357	KB 1351a
Tunnel meter[a]	14.600	16.650	10.035	13.800	15.130
SiO_2	69.68	69.33	73.44	74.85	72.61
TiO_2	0.27	0.35	0.17	0.14	0.38
Al_2O_3	15.14	15.59	12.15	12.19	13.26
FeO[b]	2.05	2.02	1.54	1.27	2.03
MnO	0.06	0.05	0.05	0.03	0.06
MgO	0.60	0.79	0.32	0.23	0.71
CaO	2.19	2.10	1.26	1.26	1.68
Na_2O	4.27	3.75	3.23	3.58	4.59
K_2O	3.91	4.33	4.82	4.22	1.69
P_2O_5	0.07	0.12	0.09	0.05	0.14
Total major	98.24	98.43	97.07	97.82	97.15
LOI	1.31	0.96	1.71	0.87	2.76
Total	99.55	99.39	98.78	98.69	99.91
$Na_2O + K_2O$	8.18	8.08	8.05	7.80	6.28

LOI = Loss on ignition

[a]Distance from north portal in kilometer

[b]Total iron is given as FeO

mafic minerals and that plagioclase becomes more albitic with increasing SiO_2. This is also the case for some of the trace elements such as Rb, which also depend linearly on SiO_2.

Nevertheless, some aspects of the compositional relationships among the Aar massif intrusions can be explained as effects of fractional crystallization from a granitic parent magma. The very low phosphorous of Brgr may have been caused by earlier apatite crystallization in the cAgr. Similarly, very low Ti in Brgr could be related to titanite and biotite formation in early cAgr. Very low X_{Mg} of Bt in Brgr compared to moderate X_{Mg} in Bt of cAgr are consistent

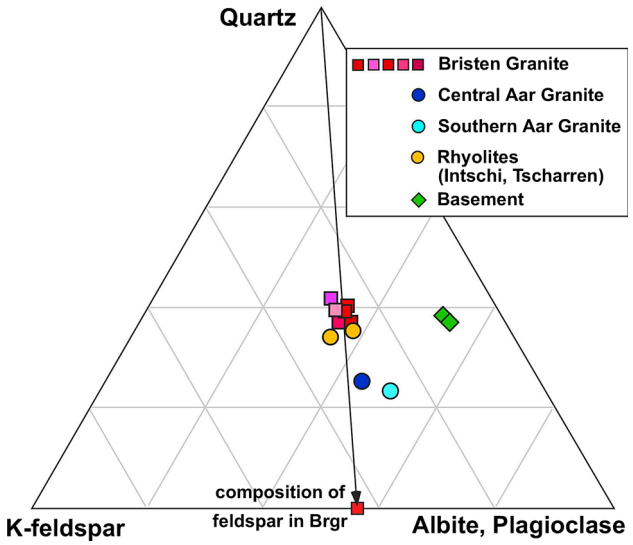

Fig. 10 Normative quartz and feldspar (vol.%) of Brgr, Permian metarhyolites, Aar granite and basement from tunnel samples (Figs. 1 and 2). Also shown is average feldspar composition of Brgr (56 Ab—44 Kfs also in vol.%)

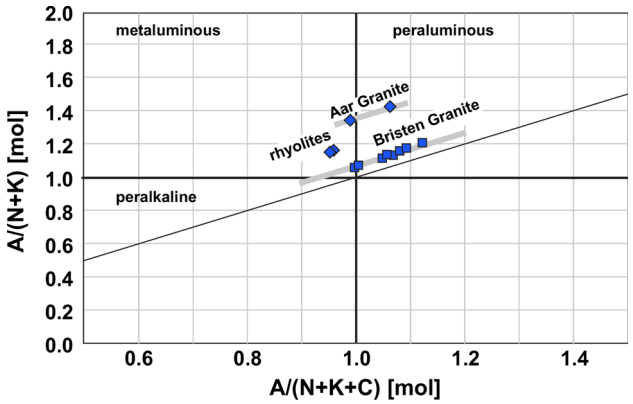

Fig. 11 Al–Na–K–Ca variation diagram (Maniar and Piccoli 1989) with data given in Tables 10 and 11 showing the mildly peraluminous character of Brgr

with a typical calc-alkaline differentiation trend (Leake 1974). Compatible trace elements such as Ba and Sr are high in cAgr and ultra-low in Brgr, which would support fractional crystallization as a possible process for the development of the magmatic suite. Sr strongly fractionates into plagioclase and Ba into K-Feldspar (Brown et al. 1984; El Bouseily and El Sokkary 1975). The Aar massif samples show a distinct differentiation trend from normal granite (cAgr) to extremely differentiated Bristen granite.

The chemical composition of granitoid rocks has been related to the tectonic environment in which they formed (e.g. De la Roche et al. 1980; Pearce et al. 1984; Harris et al. 1986; Maniar and Piccoli 1989). Particularly popular are discrimination diagrams of selected trace elements, e.g. Y-Nd and (Y + Nd)-Rb, because these elements have different abundances in the various source regions (crust, mantle) or show different behavior during processes related to the emplacement of magmas (e.g. fractionation, assimilation).

The central Aar granite shows geochemical patterns typical of late orogenic continental arc granites in accordance with its emplacement during a late Variscan orogenic stage (Schaltegger 1990). Felsic rocks may get such patterns in actual arcs, or can inherit them from whatever older source rocks melt to make them. Differentiation of Brgr from a primary Aar melt by fractional crystallization seems debatable. The fractionation of very large amounts of feldspar is not viable and inconsistent with the trace element patterns.

The composition of Brgr indicates a "within plate" (WPG) setting according to its position in various standard classification diagrams (Figs. 13 and 17). Bristen granite shows all compositional characteristics of post-orogenic granites (Maniar and Piccoli 1989) or anorogenic granites (e.g. Gopeshwor Singh and Vallinayagam 2012), low-pressure A-type granite (Vilalva and Vlach 2014) and within-plate granites (Pearce et al. 1984). Interestingly, REE- and trace element patterns of Brgr are very similar to patterns found in highly differentiated felsic rocks, so called "plagiogranites", occurring in ophiolites (Hollocher et al. 2016). The REE pattern of Bristen granite appears unrelated to the pattern of the main calc-alkaline central Aar granite. Also the trace element pattern (Fig. 14) suggests that the two types of granitoid rocks are not directly genetically related.

Remarkably, the REE pattern of Bristen granite (Fig. 16) is very similar to post-collisional late Variscan ferroan A-type granites from Sardinia (Conte et al. 2017). The about 290 Ma old main Sardinia-Corsica batholith is accompanied by slightly peraluminous F-bearing leucogranites. The chemical composition of the rocks and the annite they contain are shown to correspond to liquids generated by low degree of partial melting of different meta-igneous deep crustal sources (Conte et al. 2017). Furthermore, the Varsican main granite plutons of the Black Forest basement window are accompanied by ferroan leucogranites with compositional features similar to Bristen granite. Particularly, Wildbad granite shows a REE pattern identical to Brgr although the total REE content is much higher in the later (Möller et al. 1997). A-type leucogranites also occur in the Variscan Erzgebirge of Germany and Czechia associated with main calc-alkaline plutons (Förster et al. 1999). The Markersbach granite, for example, is a synchysite-bearing highly fractionated peraluminous A-type granite with a REE pattern almost identical to Brgr (Förster 2001). Comparable leucocratic Miocene A-type leucogranites have recently been reported from the Himalayas (Huang et al. 2017) and lower

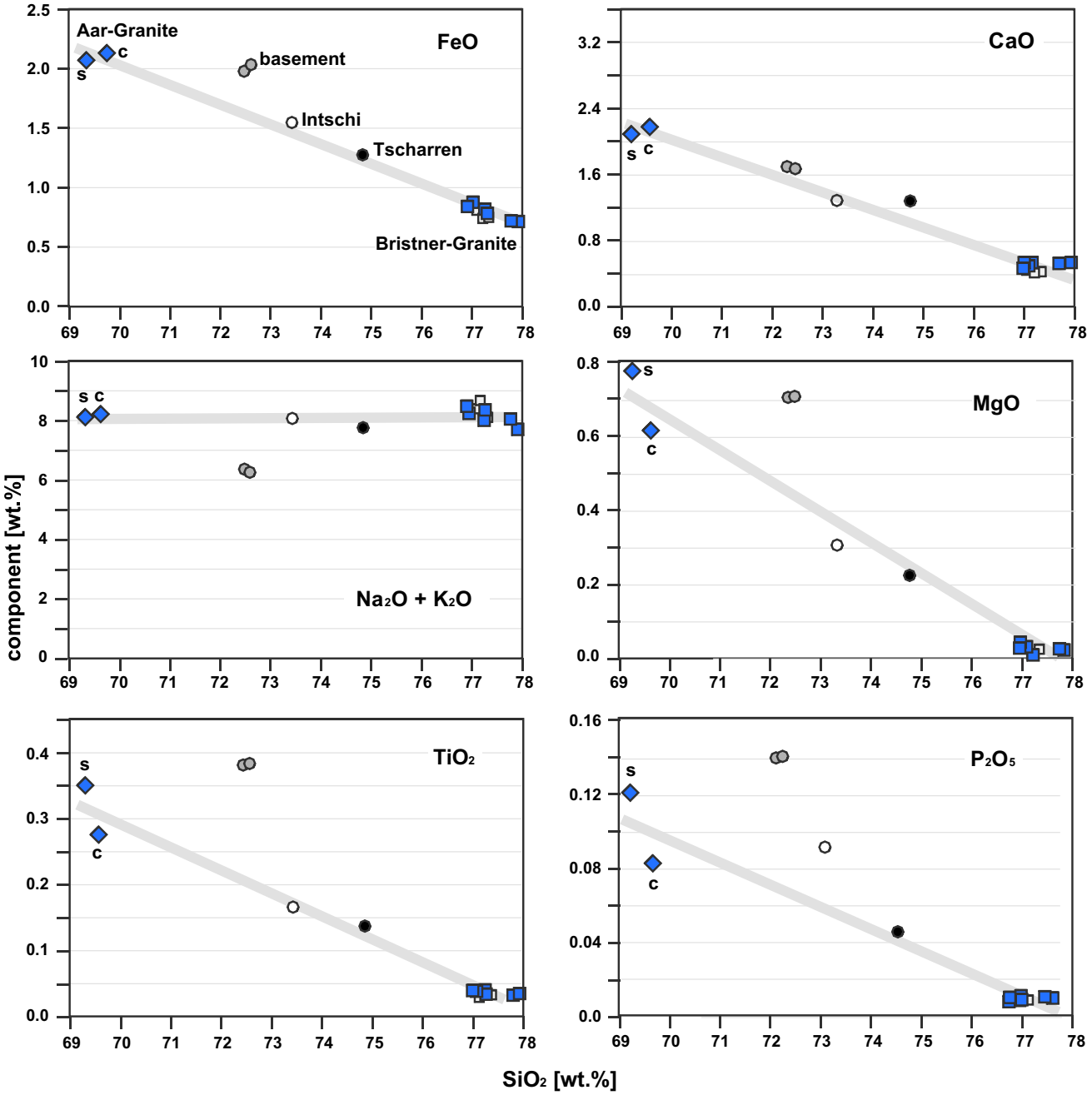

Fig. 12 Harker variation diagrams for samples of Tables 10 and 11. Squares = Bristen granite, filled circle = Tscharren formation, open circle = Intschi formation, diamonds = Aar granite (c Central Aar granite, s Southern Aar granite, gray circles = basement gneiss

Cretaceous leucogranites from the northern Zhejiang Province, South China (Hu et al. 2017). The chondrite normalized REE patterns of these granites all show a marked Eu anomaly and a slight but steady decrease towards Lu in contrast to the European Variscan leucogranites including Brgr (Fig. 16).

In addition, the composition of the bulk Bristen granite and of its mesoperthite feldspar is very similar to the compositional features of inclusions of granitic melt in garnet of the Ojen metatexite in southern Spain formed at 660–700 °C and 4.5–5 kbar (2 kbar) (Bartoli et al. 2016).

Feldspar and quartz represent > 95 wt. % of the major element composition of Brgr. The composition of Brgr is very close to the composition at the cotectic point in the Ab-Kfs-Qtz system at 100 MPa (Fig. 18) (Johannes and Holtz 1996; Blundy and Cashman 2001). This may indicate that the Brgr intruded the Pre-Variscan basement at very shallow depth of 3 km or less. Shallow intrusion depth is

Table 12 Trace element composition of Bristen granite (Brgr), central Aar granite (cAgr), southern Aar granite (sAgr), Permian rhyolites (Intschi zone, Tscharren zone) and pre-Variscan Basement (ppm)

Unit	Brgr	Brgr	Brgr	Brgr	Brgr	Brgr	Brgr	Brgr	CAgr	SAgr	Intschi	Tscharren	Basement	Detection
Sample	1348a	1361a	1362	1350	1363	1364	1349	1365	1366	1367	1356	1357	1351a	limit
Tm[a]	8.438	8.544	8.610	8.745	8.745	8.770	8.868	8.868	14.600	16.650	10.035	13.800	15.130	ppm
Ba	< 10	19	27	30	21	14	40	45	1568	1039	438	435	302	10
Sr	< 10	11	15	14	11	13	13	17	177	381	92	97	172	10
Pb	29	37	26	27	28	31	32	28	12	48	30.8	32.3	19	5
Rb	380	498	387	365	356	370	356	357	95.4	219	144	212	128	0.2
Nb	72	63	46	37	47	62	38	29	13	17	0.1	3	8	1
Ta	8.8	6.2	6.7	4.5	4.9	7.7	5.1	4.6	2.7	2.8	1.2	1.4	1.4	0.5
Th	40.2	35.7	41.5	29.3	39.2	45.6	30.6	41.3	17	24.4	21.2	23.3	11.5	0.1
U	30.1	22.9	21.9	16	20.4	28.8	17.8	23.1	5.18	11.7	6.16	7.19	15.2	0.05
Y	116	122	106	69.4	79.8	131	77	77.1	19.7	15.6	26.4	30.6	31.2	0.5
Zr	139	118	93.6	64	87.2	101	85.9	80.4	202	200	140	149	143	0.5
Hf	9	6	5	4	5	6	5	4	5	5	5	5	4	1
Be	10	9	< 5	9	7	8	8	7	< 5	6	< 5	< 5	8	5
Li	5.9	24	23	8.8	11	12	6.3	11	13	49	13	10	19	1
Cr	23	19	16	< 10	11	21	< 10	15	14	25	< 10	< 10	24	10
Ni	17	4		20	11	4	10	3	7	7	< 5	< 5	11	5
Sc	8	8	7	6	5	8	6	5	< 5	< 5	< 5	5	8	5
V	< 5	< 5	< 5	< 5	< 5	5	< 5	< 5	16	27	9	10	15	5
Zn	14	15	7	29	10	14	30	39	33	47	24	31	50	5
Co	< 0.5	< 0.5	< 0.5	< 0.5	< 0.5	< 0.5	< 0.5	< 0.5	2.5	3.5	1.5	1.5	2.2	0.5
Cs	3.8	12.3	3.6	5	5	6.5	5.3	5.2	1.6	12.3	2	6.4	3.3	1

REE are listed in Table 13

[a]Tm Distance from north portal in kilometer

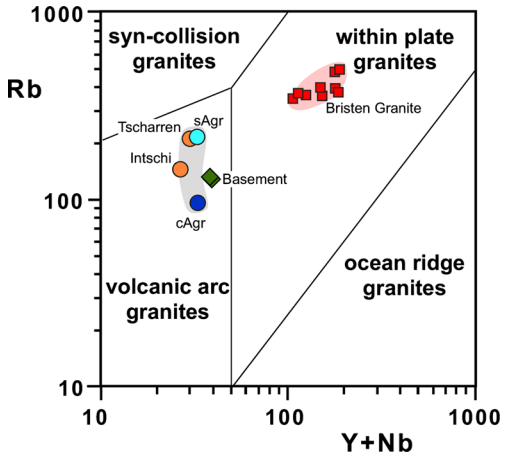

Fig. 13 Y + Nd versus Rb (ppm) discrimination diagram (Pearce et al. 1984) for the Gotthard tunnel rocks

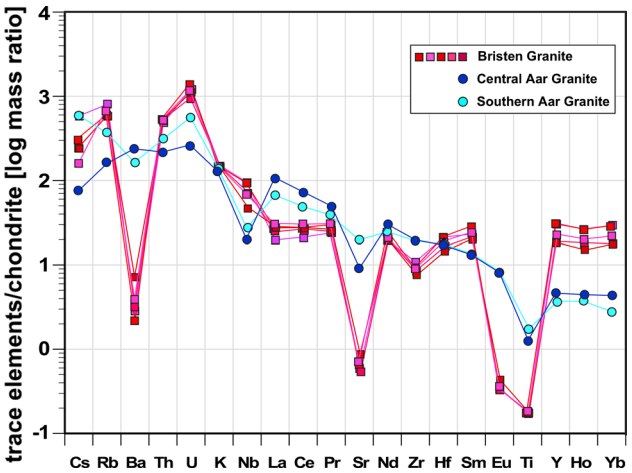

Fig. 14 Multiple trace element diagram (spider diagram). Bristen granite samples in red colors, Aar granite in blue. Primitive mantle data for normalization from McDonough and Sun (1995)

supported by the compositional features of Brgr feldspars (Parsons et al. 2005). The coarse pure K-feldspar with its massive exsolution patches of pure albite (Figs. 4 and 6b) suggests that at solidus one homogeneous feldspar formed from the cotectic melt (Kfs 44–Ab 53–An 3). The pure albite and pure K-feldspar that are present in Brgr today formed during Alpine recrystallization at lower greenschist facies conditions (~ 300 °C) and do not relate to the

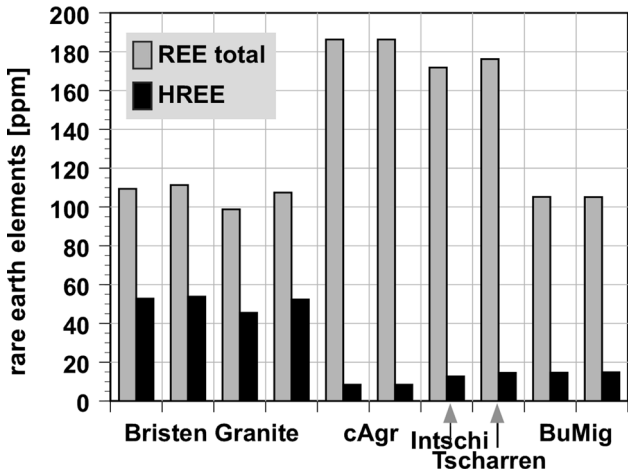

Fig. 15 Total REE and total HREE (ppm) in Gotthard tunnel rocks. A high proportion of REE in Bristen granite are HREE, cAgr contains more total REE but predominantly LREE

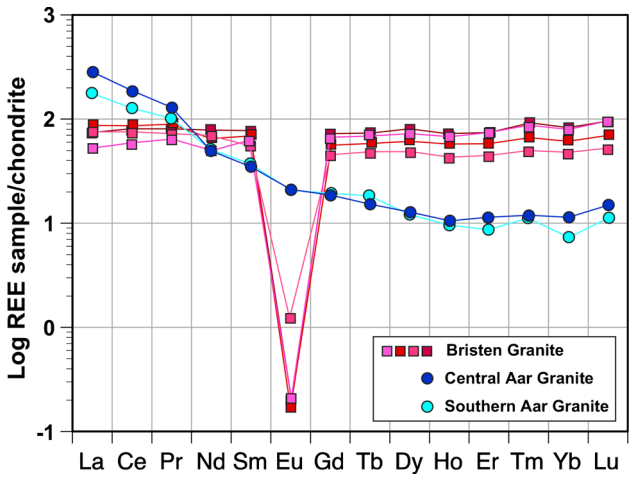

Fig. 16 Chondrite-normalized REE patterns. Bristen granite samples in red, Aar granite in blue. Chondrite data for normalization from McDonough and Sun (1995)

homogeneous ternary feldspar that originally crystallized from the residual melt at the cotectic point.

The shallow intrusion of the Brgr stock into pre-Variscan basement (Fig. 2) possibly caused contact metamorphic effects in the basement. However, the small dimension ($\sim$ 600 m) and the low solidus temperature has been insufficient for recognizable effects in the basement. Contact effects have not been observed in the tunnel. Yet, contact metamorphic effects have been reported from the basement at the contacts to the Mittagflue leucogranite (Fig. 1) further west of the Reuss valley (Schenker and Abrecht 1987). Andalusite and cordierite formed in basement schists by the thermal effects of the granite intrusion of about 5 × 3 km surface outcrop. The reported assemblages suggest a shallow intrusion also for this young granite of the Aar massif.

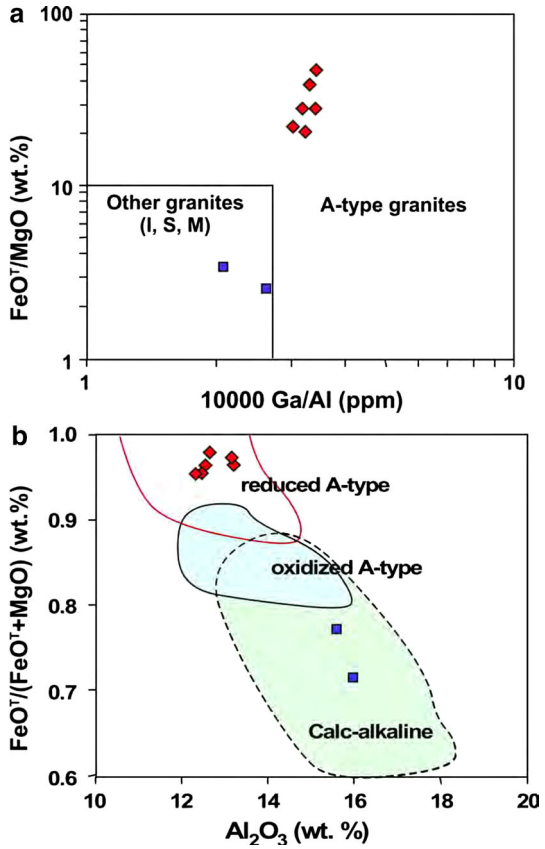

Fig. 17 Discrimination diagrams showing the reduced A-type character of Bristen granite: **a** FeO/MgO vs. Ga/Al (Whalen et al. 1987); **b** FeO/(FeO + MgO) vs. Al_2O_3 (Dall'Agnol and Oliveira 2007). Brgr red diamonds, Aar granite blue squares

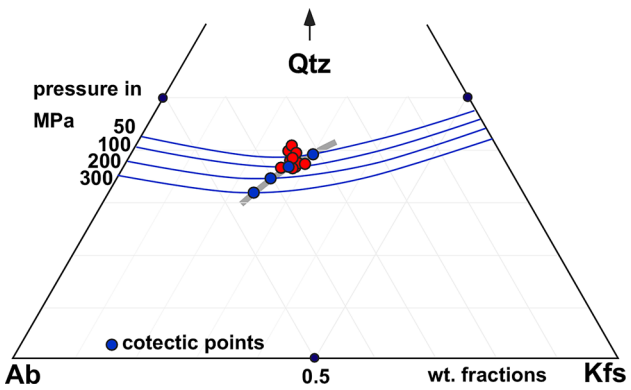

Fig. 18 Cotectic points in the system Qtz-Ab-Kfs (Blundy and Cashman 2001). Bristen granite samples (in red) cluster around the cotectic point at 100 MPa. Units = weight fractions

9.2 F-Nb-Y-REE minerals of the Bristen granite, reactions and significance

The occurrence of matrix fluorite and the incorporation of considerable amounts of F into the biotite of the Bristen granite (Table 2; Seelig and Bucher 2010) indicate a partial

Table 13 Rare Earth Element (REE) composition of Bristen granite (Brgr), central Aar granite (cAgr) and southerm Aar granite (sAgr) (ppm)

Sample KB	1361	1362	1363	1364	1365	1366	1367
Unit	Brgr	Brgr	Brgr	Brgr	Brgr	cAgr	sAgr
Tm[a]	8.544	8.61	8.745	8.77	8.868	14.600	16.65
La	13.1	20.8	16.2	16.8	17.6	67.8	42.8
Ce	37.2	55.2	41.5	47.6	44.7	117	79.7
Pr	6.05	8.46	6.25	7.57	6.51	12.5	9.66
Nd	24	31.6	23.4	29.6	24.2	37.2	30.6
Sm	9.6	10.5	8.2	11.4	8.1	5.4	5.6
Eu	0.05	0.05	0.05	0.05	0.07	1.21	1.21
Gd	12.6	12	9.17	14	8.8	3.85	3.88
Tb	2.53	2.25	1.78	2.7	1.68	0.58	0.66
Dy	17.9	16	12.7	19.1	11.8	3.32	3.05
Ho	3.71	3.29	2.54	3.9	2.26	0.63	0.54
Er	11.3	9.76	7.74	12.2	7.03	1.85	1.41
Tm	2.04	1.73	1.34	2.24	1.22	0.3	0.28
Yb	12.5	10.5	7.9	13.2	7.5	1.9	1.2
Lu	2.25	1.81	1.36	2.28	1.27	0.38	0.28
REE total	154.83	183.95	140.13	182.64	142.74	253.92	180.87
LREE	102.6	138.61	104.77	127.02	109.98	244.96	173.45
HREE	52.23	45.34	35.36	55.62	32.76	8.96	7.42
HREE %	33.7	24.6	25.2	30.5	23.0	3.5	4.1

Other trace elements are listed in Table 12

[a]Tm Distance from north portal in kilometer; Detection limits (ppm): Ce, La, Nd, Sm, Yb = 0.1; all other 0.05

pressure of HF at the solidus sufficiently high for driving the reaction:

$$(CaAl_2Si_2O_8 + KAlSi_3O_8 + 2\,FeCl_2 + 4\,HF)_{melt} = CaF_2 + 3\,SiO_2 + KFe_2Al_3Si_2O_{10}(F)_2 + 4\,HCl. \quad (1)$$

Reaction (1) combines feldspar-components and iron in the residual melt thereby forming fluorite and biotite. Euhedral primary fluorite (Fig. 7a) may have formed by reaction (1). Biotite formed by reaction (1), developed from a very late liquid strongly enriched in incompatible elements. Its later hydrothermal alteration produced the wealth of different niobates and Y-REE minerals present in Brgr. The late Alpine hydrothermal alteration is also responsible for unusually high Li in the Bristen granite and in groundwater derived from it (Wanner et al. 2017).

Below solidus anhedral late fluorite (Fig. 7c) developed together with muscovite from the reaction of feldspar with HF (Dolejs and Baker 2004),

$$CaAl_2Si_2O_8 + KAlSi_3O_8 + 4\,HF = CaF_2 + 2\,SiO_2 + KAl_3Si_3O_{10}(F)_2 + 2\,H_2O. \quad (2)$$

Reaction (2) is characteristic of the first reactions after cooling below the solidus at 700 °C suggested by the fine-grained muscovite along grain boundaries and feldspar twins together with Y- and Y-REE-fluorite partly overgrowing earlier fluorite (Figs. 4b, c and 5c). The progress of reaction (2) could relate to Variscan cooling. However, it is possible that the secondary fluorite formed during Alpine low-grade metamorphism and brittle deformation of the Brgr. This preferred interpretation is supported by the presence of pink Y-fluorite and synchysite in Alpine fissures in the granite and nearby gneisses.

Synchysite is occasionally found in late Alpine fissures of the Aar massif (Stalder et al. 1998). Its presence as euhedral crystals in late open fracture systems suggests that it formed from hydrothermal aqueous solutions during uplift, similar to the zeolite minerals found in the fissures of the Aar massif (Weisenberger and Bucher 2010). Synchysite in Bristen granite is texturally related to late fluorite and late mica-calcite veinlets (Fig. 7). The textures indicate that synchysite formed from Y-REE-bearing fluorite by reactions of the type:

$$Ca(Y,REE)F_5 + 2\,CO_2 + 2\,H_2O = Ca(Y,REE)(CO_3)_2F + 4\,HF. \quad (3)$$

It may also form from fluorite plus calcite as suggested by the assemblage found in small veinlets where abundant calcite and mica is associated with small irregularly shaped grains of synchysite. The rare parisite ($Ca(Y,REE)_2(CO_3)_3F_2$) grains intergrown with synchysite formed by reactions analogous to (3).

The rock contains an unknown number of different minerals containing Y and REE without or with variable amounts of Nb and Ti. Some of these minerals also contain Th and U as additional elements and are metamict materials rather than minerals. Many of the analyzed grains belong to the fergusonite family of Y-REE niobates. Some grains may have formed originally as euxenite or polycrase type Y-REE niobates. Some analyzed grains suggests compositions similar to yttrocolumbite or uranocolumbite. The niobates generally form extremely small droplet shaped grains of one to some μm in diameter. Quantitative uncontaminated analysis by the EPMA is difficult or impossible. Thus the assignment of the analyses to specific minerals is tentative here. Nevertheless, the Y-REE niobates occur as secondary alteration products of the biotite to chlorite + muscovite transformation during Alpine metamorphism. The heavy elements appear to be present in the primary igneous biotite where they originally have been taken up from the highly differentiated residual melt. The elements cannot be incorporated in newly formed chlorite and muscovite and form tiny grains of "leftover" material consisting of Y-REE-Nb-U oxides with various stoichiometries.

Other primary sources of Y-REE includes allanite (Gieré and Sorensen 2004; Uher et al. 2015). However, allanite is very rare in Brgr and the textures support biotite as a prime source of the elements of the various niobates (Figs. 5 and 6). Phosphates such as monazite or xenotime, another potential source of Y-REE in secondary minerals (Grapes et al. 2005) have not been found in Brgr.

Thorite ($(Th,U)SiO_4$) occurs as discrete very small grains typically associated with much larger zircon ($(Zr,Hf)SiO_4$) and appears to be a product of unmixing rather than primary igneous as in many A-type granites (Charoy and Raimbault 1994). The thorite always contains a considerable amount of coffinite component.

10 Summary and conclusion

The fine-grained leucocratic Bristen granite is strongly depleted in TiO_2, P_2O_5, MgO, Sr, and Ba and enriched in Rb, Th, U, Nb, Y, and F. The major and trace element composition of Bristen granite, suggests that Brgr does not belong to an evolution sequence including cAgr and other Variscan intrusives of the Aar massif evolving from normal calc-alkaline granites to leucogranites and finally to aplitic granites. The Bristen granite is the most differentiated and evolved rock of the Variscan granites of the Aar massif and formed from a melt emplaced as a small stock at in the shallow upper crust (3 km). The melt formed by local partial melting of pre-Variscan gneiss in the lower crust. Melts with Brgr REE and trace element patterns may form by low degree of partial melting during migmatization of lower crustal material (Bartoli et al. 2016).

However, the composition of the residual melt from which Brgr formed shows the effects of fractional crystallization indicated for example by a marked Eu-anomaly in the REE-pattern of the Brgr. Furthermore, progressing fractionation concentrates Sr and Ba in plagioclase and K-feldspar at early stages, removing these elements from the residual melt. Rubidium strongly accumulates during the fractionation process in the residual melts and finally Rb became the characteristic incompatible element of the Bristen granite. During late stages of crystallization of the Bristen granite from residual melt igneous fluorite formed together with biotite from anorthite and K-feldspar component.

The Alpine metamorphic and hydrothermal overprint under lower greenschist facies conditions mainly transformed igneous biotite to chlorite and muscovite. This transformation produced a wealth of secondary product minerals including Y- and REE-rich fluorite, synchysite, parisite, thorite, fergusonite, and other Y-REE-rich Nb–Ti oxides.

Acknowledgements We would like to thank AlpTransit Gotthard AG for providing access to the tunnel. The generous support by the tunnel geologists Beat Frei and Thomas Breitenmoser providing rock and water samples is gratefully acknowledged. We are grateful to Peter Amacher for contributing data on the Alpine fissure minerals from the tunnel to the present study. Special thanks go to all technicians of the Mineralogy and Geochemistry laboratories of the University of Freiburg. Peter Hayoz from Swisstopo, Wabern, supported this study by providing fresh core samples of the granites. We gratefully acknowledge the constructive reviews by Christian Gisler and an anonymous reviewer and the efficient editorial handling by Edwin Gnos.

References

Abrecht, J., & Schaltegger, U. (1988). Aplitic intrusions in the Central Aar massif basement: geology, petrography and Rb/Sr data. *Eclogae Geologicae Helvetiae, 81,* 227–239.

Amacher, P., & Schüppach, T. (2011). *NEAT-Mineralien, Kristall-Schätze tief im Berg* (p. 233). Amsteg: Verlag GEO-Uri.

Anderson, I. C., Frost, C. D., & Frost, B. R. (2003). Petrogenesis of the Red Mountain pluton, Laramie anorthosite complex, Wyoming: implications for the origin of A-type granite. *Precambrian Research, 124,* 243–267.

Armbruster, T., Kohler, T., Meisel, T., Nägler, T. F., Götzinger, M. A., & Stalder, H. A. (1996). The zeolite, fluorite, quartz assemblage of the fissure at Gibelsbach, Fiesch (Valais, Switzerland): crystal chemistry, REE patterns, and genetic speculations. *Schweizerische Mineralogische und Petrographische Mitteilungen, 76,* 131–146.

Bartoli, O., Acosta-Vigil, A., Ferrero, S., & Cesare, B. (2016). Granitoid magmas preserved as melt inclusions in high-grade metamorphic rocks. *American Mineralogist, 101,* 1543–1559.

Berger, A., Mercolli, I., Herwegh, M., & Gnos, E. (2017). *Geological Map of the Aar Massif* (p. 129). Geological Special Map: Tavetsch and Gotthard Nappes.

Blundy, J., & Cashman, K. (2001). Ascent-driven crystallisation of dacite magmas at Mount St Helens, 1980–1986. *Contrib. Mineral. Petrol., 140,* 631–650.

Breitschmid, A. (1982). Diagenese und schwache Metamorphose in den sedimentaren Abfolgen der Zentralschweizer Alpen. *Eclogae Geologicae Helvetiae, 75,* 331–380.

Brown, G. C., Thorpe, R. S., & Webb, P. C. (1984). The geochemical characteristics of granitoids in contrasting arcs and comments on magma sources. *Journal of the Geological Society, 141,* 413–426.

Bucher, K., & Frost, B. R. (2006). Fluid transfer in high-grade metamorphic terrains intruded by anorogenic granites: the Thor Range, Antarctica. *Journal of Petrology, 47,* 567–593.

Charoy, B., & Raimbault, L. (1994). Zr-, Th-, and REE-rich biotite differentiates in the A-type granite pluton of Suzhou (Eastern China): the key role of fluorine. *Journal of Petrology, 35,* 919–962.

Conte, A. M., Cuccuru, St, D'Antonio, M., Naitza, St, Oggiano, G., Secchi, F., et al. (2017). The post-collisional late Variscan ferroan granites of southern Sardinia (Italy): Inferences for inhomogeneity of lower crust. *Lithos, 294–295,* 263–282.

Dall'Agnol, R., & Oliveira, D. C. (2007). Oxydized, magnetite-series, rapakivi-type granites of Carajas, Brazil: implications for classification and petrogenesis of A-type granites. *Lithos, 93,* 215–233.

De la Roche, H., Leterrier, J., Grandclaude, P., & Marchal, M. (1980). A classification of volcanic and plutonic rocks using R1R2-diagram and major-element analyses— its relationships with current nomenclature. *Chemical Geology, 29,* 183–210.

Dolejs, D., & Baker, D. R. (2004). Thermodynamic analysis of analysis of the system Na_2O-K_2O-CaO-Al_2O_3-SiO_2-H_2O-F_2O_{-1}: stability of fluorine-bearing minerals in felsic igneous suites. *Contributions to Mineralogy and Petrology, 146,* 762–778.

Duran, C. J., Seydoux-Guillaume, A.-M., Bingen, B., Gou, S., de Parseval, P., Ingrin, J., et al. (2016). Fluid-mediated alteration of (Y, REE, U, Th)–(Nb, Ta, Ti) oxide minerals in granitic pegmatite from the Evje-Iveland district, southern Norway. *Mineralogy and Petrology, 110,* 581–599.

El Bouseily, A. M., & El Sokkary, A. A. (1975). The relation between Rb, Ba and Sr in granitic rocks. *Chemical Geology, 16,* 207–219.

Finger, F., & Steyrer, H. P. (1990). I-Type granitoids as indicators of a late Paleozoic convergent ocean continent margin along the southern flank of the central European Variscan orogen. *Geology, 18,* 1207–1210.

Förster, H.-J. (2001). Synchysite-(Y)—synchysite-(Ce) solid solutions from Markersbach, Erzgebirge, Germany: REE and Th mobility during high-T alteration of highly fractionated aluminous A-type granites. *Mineralogy and Petrology, 72,* 259–280.

Förster, H.-J., Tischendorf, G., Turnbull, R. B., & Gottesmann, B. (1999). Late-collisional granite magmatism in the Variscan Erzgebirge, Germany. *Journal of Petrology, 40,* 1613–1645.

Frey, M. (1987). The reaction-isograd kaolinite + quartz = pyrophyllite + H_2O, Helvetic Alps, Switzerland. *Schweizer Mineralogische und Petrographische Mitteilungen, 67,* 1–11.

Frey, M., Bucher, K., Frank, E., & Mullis, J. (1980). Alpine metamorphism along the Geotraverse Basel-Chiasso— a review. *Eclogae Geologicae Helveticae, 73,* 527–546.

Geyer, M., Nitsch, E., Simon, Th, Geyer, O. F., & Gwinner, M. P. (2011). *Geologie von Baden-Württemberg* (5th ed., p. 627). Stuttgart: Schweizerbart.

Gieré, R., & Sorensen, S. S. (2004). Allanite and other REE-rich epidote-group minerals. *Reviews in Mineralogy and Geochemistry, 56,* 431–493. https://doi.org/10.2138/gsrmg.56.1.431

Gopeshwor Singh, L., & Vallinayagam, G. (2012). Petrological and geochemical constraints in the origin and associated mineralization of A-type granite suite of the Dhiran Area, Northwestern Peninsular India. *Geosciences, 2,* 66–80.

Grapes, R., Bucher, K., & Hoskin, P. W. O. (2005). Monazite-epidote reaction in amphibolite grade blackwall rocks. *European Journal of Mineralogy, 17,* 553–566.

Guntli, P., Keller, F., Lucchini, R. and Rust, S. (2016). Gotthard-Basistunnel: geologie, geotechnik, hydrogeologie—zusammenfasender Schlussbericht. Berichte der Landesgeologie Nr.7 pp.180. Bundesamt für Landestopografie (swisstopo), Wabern, Switzerland.

Hanson, S. L., Simmons, W. B., Webber, K. L., & Falster, W. U. (1992). Rare-earth-element mineralogy of granitic pegmatites in the Trout Creek Pass district, Chaffee county, Colorado. *Canadian Mineralogist, 30,* 673–686.

Harris, N. B. W., Pearce, J. A., & Tindle, A. G. (1986). Geochemical characteristics 497 of collision-zone magmatism. In M. P. Coward & A. C. Ries (Eds.), *Collision tectonics* (Vol. 19, pp. 67–81). London: Geological Society Special Publication.

Hollocher, K. (2007). Calculation of a CIPW norm from a bulk chemical analysis. Geology Department, Union College, Schenectady, NY, 12308, USA. http://www.union.edu/PUBLIC/GEODEPT/COURSES/petrology/norms.htm. Accessed 15 Mar 2016.

Hollocher, K., Robinson, P., Seaman, K., & Walsh, W. (2016). Ordovician-Early Silurian intrusive rocks in the northwest part of the Upper Allochthon, Mid-Norway: Plutons of an Iapetan Volcanic Arc Complex. *American Journal of Science, 316,* 925–980.

Hu, Q., Yu, K., Liu, W., Hu, Z., & Zong, K. (2017). The 131–134 Ma A-type granites from northern Zhejiang Province, South China: implications for partial melting of the Neoproterozoic lower crust. *Lithos, 294–295,* 39–52.

Huang, Ch., Zhao, Z., Li, G., Zhua, D., Liua, D., & Shi, Q. (2017). Leucogranites in Lhozag, southern Tibet: implications for the tectonic evolution of the eastern Himalaya. *Lithos, 294–295,* 246–262.

Hügi, T. (1956). Vergleichende petrologische und geochemische Untersuchungen an Graniten des Aarmassivs. In: *Beiträge zur Geologischen Karte der Schweiz* (vol. N.F., 94, p. 86). Bern: Kümmerly and Frey AG, Geographischer Verlag.

Irber, W. (1999). The lanthanide tetrad effect and its correlation with K/Rb, Eu/Eu*, Sr/Eu, Y/Ho, and Zr/Hf of evolving peraluminous granite suites. *Geochimica et Cosmochimica Acta, 63,* 489–508.

Izett, G. A. (1981). Volcanic ash beds: recorders of Upper Cenozoic silicic pyroclastic volcanism in the western United States. *Journal of Geophysical Research, 86,* 10200–10222.

Jahn, B.-M., Wu, F., Capdevilla, R., Martineau, F., Zhao, Z., & Wang, Y. (2001). Highly evolved juvenile granites with tetrad REE patterns: the Woduhe and Baerzhe granites from the the Great Xing'an Moubtains in NE China. *Lithos, 59,* 171–198.

Johannes, W., & Holtz, F. (1996). *Petrogenesis and experimental petrology of granitic rocks* (p. 335). Heidelberg: Springer.

Keppie, J. D. (1994). *Pre-Mesozoic geology in France and related areas* (p. 536). Berlin Heidelberg: Springer.

Labhart, T. P. (1977). Aarmassiv und Gotthardmassiv. In M. P. Gwinner (Ed.), *Sammlung Geologischer Führer* (Vol. 63, p. 173). Berlin, Stuttgart: Gebrüder Borntraeger.

Labhart, T. P. (2005). *Geologie der Schweiz* (p. 211). Bern: Ott Verlag.

Leake, B. E. (1974). The crystallization history and mechanism of emplacement of the western part of the Galway Granite, Connemara, Western Ireland. *Mineralogical Magazine, 39,* 498–512.

Maniar, P. D., & Piccoli, P. M. (1989). Tectonic discrimination of granitoids. *Geological Society of America Bulletin, 101,* 635–643.

McCann, T., Mader, H. M., & Coles, S. G. (2008). *The Geology of Central Europe, vol 1 Precambrian and Palaeozoic* (p. 784). London: The Geological Society of London.

McDonough, W. F., & Sun, S. S. (1995). The composition of the Earth. *Chemical Geology, 120,* 223–253.

Mercolli, I., & Oberhänsli, R. (1988). Variscan tectonic evolution in the Central Alps: a working hypothesis. *Schweizerische Mineralogische und Petrographische Mitteilungen, 68,* 491–500.

Möller, P., Stober, I., & Dulski, P. (1997). Seltenerdelement-, Yttrium-Gehalte und Bleiisotope in Thermal- und Mineralwässern des Schwarzwaldes.-. *Grundwasser, 3*(2), 118–132.

Monecke, T., Kempe, U., Monecke, J., Sala, M., & Wolf, D. (2002). Tetrad effect in rare earth element distribution patterns: a method of quantification with application to rock and mineral samples from granite-related rare metal deposits. *Geochimica et Cosmochimica Acta, 66,* 1185–1196.

Oberhänsli, R., Schenker, F., & Mercolli, I. (1988). Indications of Variscan nappe tectonics in the Aar Massif. *Schweizerische Mineralogische und Petrographische Mitteilungen, 68,* 509–520.

Parsons, I., Thompson, P., Lee, M. R., & Cayzer, N. (2005). Alkali feldspar microtextures as provenance indicators in siliciclastic rocks and their role in feldspar dissolution during transport and diagenesis. *Journal of Sedimentary Research, 75,* 921–942.

Pearce, J. A., Harris, N. B. W., & Tindle, A. G. (1984). Trace element discrimination diagrams for the tectonic interpretation of granitic rocks. *Journal of Petrology, 25,* 956–983.

Pfiffner, O. A. (2014). *Geology of the Alps* (2nd edn., 368 pp.). Chichester: Wiley Blackwell.

Pflugshaupt, P. (1927). Beiträge zur Petrographie des östlichen Aarmassifs—Petrographisch geologische Untersuchungen im Gebiete des Bristenstockes. *Schweizerische Mineralogische und Petrographische Mitteilungen, 7,* 321–378.

Pouchou, J. L., & Pichoir, F. (1984). "PAP" (φ-ρ-z) correction procedure for improved quantitative microanalysis. In J. T. Armstrong (Ed.), *Microbeam Analysis* (pp. 104–106). California: San Francisco Press.

Schaltegger, U. (1990). The Central Aar Granite: highly differentiated calc-alkaline magmatism in the Aar Massif (Central Alps, Switzerland). *European Journal of Mineralogy, 2,* 245–259.

Schaltegger, U. (1993). The evolution of the polymetamorphic basement in the Central Alps unravelled by precise U-Pb zircon dating. *Contributions to Mineralogy and Petrology, 113,* 466–478.

Schaltegger, U. (1994). Unravelling the pre-Mesozoic history of the Aar and Gotthard massifs (Central Alps) by isotopic dating—a review. *Schweizerische Mineralogische und Petrographische Mitteilungen, 74,* 41–51.

Schaltegger, U., & Corfu, F. (1992). The age and source of late Hercynian magmatism in the central Alps: evidence from precise U-Pb ages and initial Hf isotopes. *Contributions to Mineralogy and Petrology, 111,* 329–344.

Schaltegger, U., & Corfu, F. (1995). Late Variscan "Basin and Range" magmatism and tectonics in the Central Alps: evidence from U-Pb geochronology. *Geodinamica Acta, 8,* 82–98.

Schaltegger, U., Gnos, E., Küpfer, T., & Labhart, T. P. (1991). Geochemistry and tectonic significance of Late Hercynian potassic and ultrapotassic magmatism in the Aar massif (Central Alps). *Schweizerische Mineralogische und Petrographische Mitteilungen, 71,* 391–403.

Schenker, F., & Abrecht, J. (1987). Prä-aargranitische Anatexis, variszische Kontaktmetamorphose und alpidische Regionalmetamorphose im Oberhasli (zentrales Aarmassiv, Schweiz). *Schweizerische Mineralogische und Petrographische Mitteilungen, 67,* 13–26.

Seelig, U., & Bucher, K. (2010). Halogens in water from the crystalline basement of the Gotthard rail base tunnel (Central Alps). *Geochimica Cosmochimica Acta, 74,* 2581–2595.

Smith, D. R., Noblett, J., Wobus, R. A., Unruh, D., Dougalss, J., Beane, R., et al. (1999). Petrolgoy and geochemistry of late-stage intrusions of the A-type, mid-Proterozoic Pikes Peak batholith (Central Colorado, USA): implications for petrogenetic models. *Precambrian Research, 98,* 271–305.

Stalder, H. A. (1964). Petrographische und mineralogische Untersuchungen im Grimselgebiet. *Schweizerische Mineralogische und Petrographische Mitteilungen, 44,* 187–398.

Stalder, H. A., Wagner, A., Graeser, S., & Stuker, P. (1998). *Mineralienlexikon der Schweiz* (p. 608). Wepf: Basel.

Uher, P., Ondrejka, M., Bačík, P., Broska, I., & Konečný, P. (2015). Britholite, monazite, REE carbonates, and calcite: products of hydrothermal alteration of allanite and apatite in A-type granite from Stupné, Western Carpathians, Slovakia. *Lithos, 236–237,* 212–225.

Vilalva, F. C. J., & Vlach, S. R. F. (2014). Geology, petrography and geochemistry of the A-type granites from the Morro Redondo Complex (PR-SC), southern Brazil, Graciosa Province. *Annals of the Brazilian Academy of Sciences, 86,* 85–116.

Von Raumer, J., Abrecht, J., Bussy, F., Lombardo, B., Menot, R.-P., & Schaltegger, U. (1999). The Palaeozoic metamorphic evolution of the Alpine External Massifs. *Schweizerische Mineralogische und Petrographische Mitteilungen, 79,* 5–22.

Wang, R.-C., Wang, D.-Z., Zhao, G.-T., Lu, J.-J., Chen, X.-M., & Xu, S.-J. (2001). Accessory mineral record of magma-fluid interaction in the Laoshan I- and A-type granitic complex, Eastern China. *Physics and Chemistry of the Earth (A), 26*(9–10), 835–849.

Wanner, Ch., Bucher, K., Pogge von Strandmann, P. A. E., Waber, N. H., & Pettke, T. (2017). On the use of Li isotopes as a proxy for water-rock interaction in fractured crystalline rocks: a case study from the Gotthard rail base tunnel. *Geochimica Cosmochimica Acta, 198,* 396–418.

Weisenberger, T., & Bucher, K. (2010). Zeolites in fissures of granites and gneisses of the Central Alps. *Journal of Metamorphic Geology, 28,* 825–847.

Whalen, J. B., Currie, K. L., & Chappell, B. W. (1987). A-type granites: geochemical characteristics, discrimination and petrogenesis. *Contributions to Mineralogy and Petrology, 95,* 407–419.

Whitney, D. L., & Evans, B. W. (2010). Abbreviations for names of rock-forming minerals. *American Mineralogist, 95,* 185–187.